universität
wien

# DIPLOMARBEIT

Titel der Diplomarbeit:

## Characterisation of MuSK endocytosis at the neuromuscular synapse

angestrebter akademischer Grad

**Magistra der Naturwissenschaften (Mag. rer. nat.)**

| | |
|---|---|
| Verfasserin: | Cristina Melinte |
| Matrikel-Nummer: | 0647217 |
| Studienrichtung: | A 439-Zoologie |
| (lt. Studienblatt): | |
| Betreuer: | Ao. Univ.-Prof. Dr. Axel Schmid/ Dr. Ruth Herbst |

Wien, April 17, 2009

# Acknowledgements

First of all I want to thank Dr. Ruth Herbst for providing this interesting and promising project for my diploma thesis. I am grateful for her very best support as a supervisor, for helpful advices and answers to many questions. Moreover, I appreciate that she trained me to work independently from the very beginning. I want to thank Susan Luiskandl for the wonderful working atmosphere and for all the time she invested to teach me new things. I want to thank my lab colleagues for providing a perfect working atmosphere, for additional help and interesting discussions. Many thanks also go to Prof. Werner Sieghart and his group. Finally, I wish to thank my family and friends for their support and encouragement.

# Contents

# Chapter 1

# Zusammenfassung

Die Innervierung der Skelettmuskulatur durch Motorneurone führt zur Bildung von neuromuskulren Synapsen (NMS). Agrin, ein von Nerven sezerniertes Protein, zusammen mit Lrp4, bekannt als Agrin Rezeptor, führt zur Aktivierung der muskelspezifischen Rezeptortyrosinkinase, MuSK. Diese Aktivierung von MuSK resultiert in der Phosphorylierung von spezifischen Tyrosinen im MuSK-eigenen intrazellulären Bereich. Dieser Prozess ist essentiell für alle bekannten Aspekte post- und präsynaptischer Differenzierung, inklusive der postsynaptischen Anreichung von Acetylcholinrezeptoren (AChR). MuSK knock-out Mäuse haben keine neuromuskulären Synapsen und sterben gleich nach der Geburt aufgrund respiratorischen Versagens. AChRs und andere synaptische Proteine befinden sich gleichmässig auf der Muskelfaser verteilt. Zusammengefasst sind Agrin und MuSK Schlüsselfiguren für die Entwicklung der neuromuskulären Synapse. Die Mechanismen, die die Expression, die Stabilität und die Lokalisierung von MuSK an der Muskeloberfläche, und damit den Signalweg von MuSK beeinflussen, sind noch nicht bekannt.

Studien über andere Rezeptortyrosinkinase (RTKs) haben gezeigt, dass die Endozytose von Zelloberflächenrezeptoren die Signalwege beeinflussen können. Die Aktivierung von RTKs führt zur Aktivierung von intrazellulären Signalwegen, die wichtig für verschiedene Zellprozesse sind, wie zum Beispiel die Proliferation, Differenzierung, die Migration und das Überleben der Zellen. Liganden-induzierte Rezeptorendozytose ist für die Weitergabe und Spezifisierung von Signalen notwendig. Somit, besteht ein enger Zusammenhang zwischen Endozytose und Signalübertragung. Im Muskel sind endosomale Kompartimente reichlich unter der NMS exprimiert und daher wird die Endozytose als sehr wichtig bei der Kontrolle der postsynaptischen Rezeptordichte angesehen.

Diese Diplomarbeit hatte zum Ziel MuSK Endozytose und deren Einfluss auf Agrininduziertes AChR Clustering zu untersuchen. Mittels der Blockierung von Dynamin Funktion, könnte ich zeigen, dass die MuSK Endozytose in HeLa Zellen stark beeinträchtigt

wurde. Dies impliziert, dass Dynamin2 eine wichtige Rolle in der MuSK Endozytose spielt. Dynasore, ein chemischer Inhibitor von Dynamin, reduzierte im groen Ausma das Agrin-induzierte AChR Clustering in Muskelzellen. Dies bekräftigt, dass die Dynamin-abhängige MuSK Endozytose eine wichtige Rolle bei der Aktivierung der MuSK-spezifischen Signalwege spielt. Dynasore erwies sich als wichtiges Werkzeug bei der Blockierung von Dynamin-abhängiger Endocytose und half daher bei der Untersuchung von MuSK Endozytose und ihren Einfluss auf die Agrin-MuSK Signalwirkung. In weiteren Experimenten wurde eine Muskelzelllinie erzeugt, die getaggtes MuSK exprimiert. Die Generierung dieser Muskelzelllinie eröffnet Möglichkeiten bei der Untersuchung von MuSK-Endozytose in Muskelzellen. So kann man MuSK in lebenden Zellen markieren und dessen Wanderung in Zellen beobachten. Dadurch konnte ich mögliche Co-Lokalisationen zwischen MuSK und spezifischen endozytischen Kompartimenten visualisieren.

# Chapter 2

# Summary

The innervation of skeletal muscle by motor neurons leads to the formation of neuro-muscular synapses (NMSs). Agrin, a nerve-derived protein, together with Lrp4 known as the agrin receptor, leads to the activation of muscle-specific receptor tyrosine kinase MuSK. Phosphorylation of several tyrosine residues in the MuSK intracellular domain is essential for all known aspects of postsynaptic and presynaptic differentiation, including the postsynaptic clustering of acetylcholine receptors (AChRs).

MuSK knock-out mice fail to form NMSs, die shortly after birth due to respiratory failure and their AChRs and other synaptic proteins are uniformly expressed along the muscle fibers.

Taken together, agrin and MuSK are the key players at developing NMSs that initiate pre- and post-synaptic differentiation. Mechanisms that regulate surface MuSK expression, stability, localization and consequently influence MuSK signaling pathways are as yet unresolved. Studies on other receptor tyrosine kinases (RTKs) have shown that endocytosis and trafficking of cell surface receptors can modulate signaling pathways. Activation of RTKs leads to the induction and specification of intracellular signaling pathways which are important for cellular behaviour like proliferation, differentiation, motility and survival.

These findings demonstrate that receptor trafficking and signaling are closely linked. In the muscle, endosomal compartments are highly concentrated beneath the NMSs and endocytosis is considered to be of particular importance in the control of postsynaptic receptor density.

This study aimed to better characterize MuSK endocytosis and its influence on agrin induced AChR clustering. By blocking dynamin function I could show that MuSK endocytosis is severely affected in HeLa cells, indicating a role for dynamin in MuSK endocytosis. The dynamin inhibitor, dynasore significantly reduced agrin-induced AChR clustering in muscle cells, which supports the idea that dynamin-dependent MuSK endocytosis might

be important for agrin-MuSK signaling at the NMS. Dynasore, proved to be a powerful tool in blocking dynamin dependent endocytosis and studying MuSK endocytosis and its influence on agrin-MuSK signaling.

Another tool in studying MuSK trafficking in muscle cells was the production of a muscle cell line that expresses a tagged MuSK. This allows the labelling of MuSK in living cells and the visualisation of trafficking processes. This cell line will allow a better characterisation of MuSK endocytosis in muscle cells.

# Chapter 3

# Introduction

## 3.1 The neuromuscular synapse

The neuromuscular junction (NMJ) also called neuromuscular synapse (NMS) represents the contact side between the axon terminal of a motor neuron and a muscle fiber. This excitable region of the muscle fiber plasma membrane is named motor end plate. A mature and functional NMS is an anatomical and physiological key element in the process of muscle contraction. The nervous impulse initiated in the center nervous system is transmitted along motor axons to the muscle fiber. The increase of Ca2+ ions in the axon terminal cytosol of the motor neuron leads to the release of neurotransmitter acetylcholine (ACh) in the synaptic cleft. ACh will diffuse and reversibly bind to nicotinic acetylcholine receptors (nAChRs) from the postsynaptic membrane. nAChRs are ligand-gated ion channels and the binding of ligand (ACh) leads to a opening of the channel and the diffusion of Na+ and K+ across the receptor pore. This causes depolarization of voltage-gated sodium channels, which allows initiation of the action potential (AP). AP is propagated along the membrane and T-tubules to the sarcoplasmic reticulum where Ca2+ will be released into the cytosol and binds to troponin-C. This causes a conformational change that moves tropomyosin out of the way so that the cross bridges can attach to actin and produce muscle contraction. A schematic representation of the motor neuron, NMS and muscle fiber is shown in figure 3.1.

## 3.2 Synaptogenesis of the neuromuscular synapse

Neuromuscular synapses are functional even before birth, but still many transformations take place to generate a mature postsynaptic apparatus from the nascent AChR cluster. A fully mature NMS is characterized by its highly folded postsynaptic membrane as well as the highly differentiated nerve terminal as shown in figure 3.1.
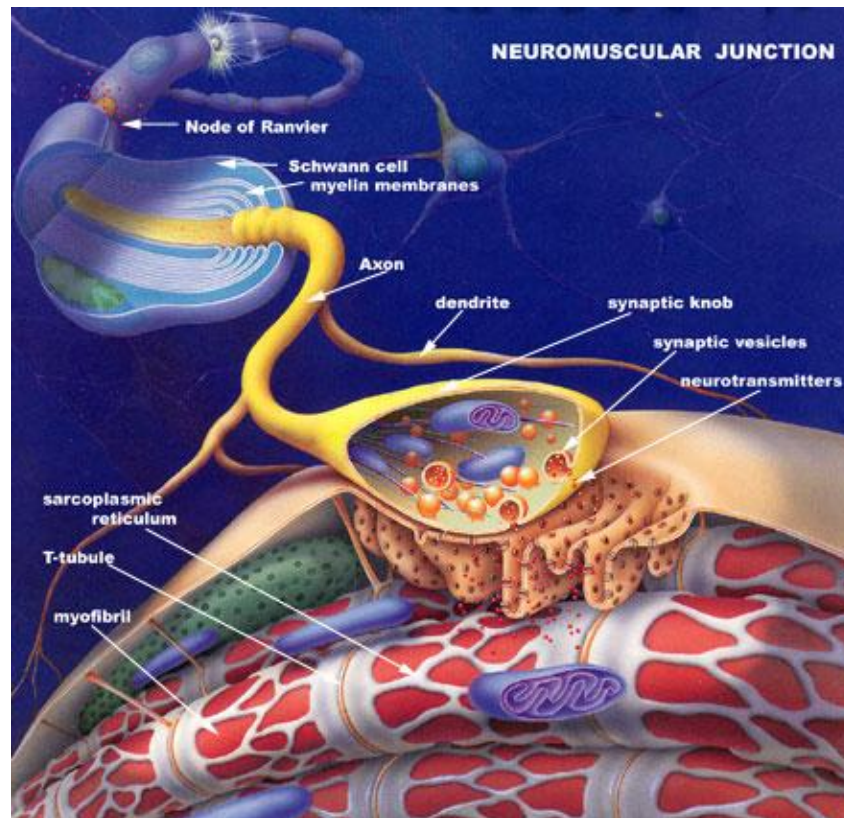
Figure 3.1: Cartoon of the motor neuron, NMS and muscle fiber. Axon terminals from a motor neuron project toward muscle; synaptic knob containing vesicles with neurotransmitters, postjunctional folds, T-tubules and sorcoplasmic reticulum are despicted (picture by Charles Mallery: fig.cox.miami.edu/ cmallery/150/neuro/muscle.htm.)
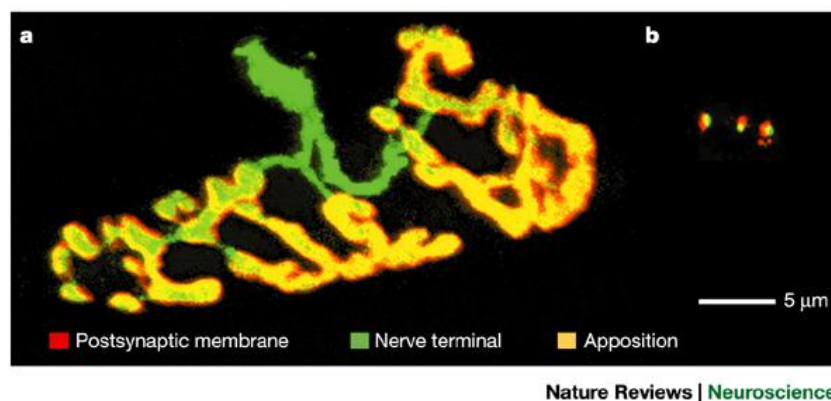


Figure 3.2: The neuromuscular junction. a — The neuromuscular junction of an adult mouse. b — Three synapses on cultured mouse hippocampal neurons shown at the same scale.In green is the motor neuron terminals and in yellow is the postsynaptin membrane (image published by Sanes and Lichtman, 2001).

AChRs are specifically concentrated at the NMS beneath the motor nerve terminal. Its density in this region is $> 10.000/\mu$ m$^2$ compared with the extrasynaptic membrane where it is $< 10/\mu$ m$^2$ [Fambrough, 1979]. The AChRs are localized exclusively at the crests of postsynaptic folds [Burden, 2002] and specific changes such as the clustering of nuclei to synaptic sites, expression of AChR mRNA in synaptic areas and suppression of AChR gene transcription in non-synaptic nuclei contribute to the establishment of a fully mature synapse [Cohen et al., 1997].

AChR subunit composition is changed as the embryonic form of AChRs containing $\gamma$-subunits is replaced by AChRs containing the homologous $\epsilon$-subunits [Numberger et al., 1991]. This results in shorter channel opening times, but the channel conductance and its Ca2+ permeability increases.

During embryonic development (embryonic day 11 in mice) myoblasts begin to fuse, forming multinucleated skeletal muscle fibers. After formation of these premature muscle fibers, growth cones of motor neurons arrive, start branching and begin to establish nerve-muscle contact (E12-E13) [Burden, 2002]. Until E14.5 few aneuraly AChR clusters are detectable, located in the center region of the muscle [Lin et al., 2001]. This phenomenon can also be observed on myotubes cultured without neurons were "spontaneous" AChR clusters, often called "hot spots" can be observed [Vogel et al., 1972, Fischbach & Cohen, 1973, Bloch, 1979]. This supports the idea that AChR clusters might form aneurally and then are recognized by the ingrowing axon. *In vivo*, the presence of nerve will lead to a redistribution of AChR clusters in a distinct region termed the endplate zone [Luo et al., 2003], a process finished at E16-E18. In a mature NMS, the initially flat postsynaptic membrane develops its characteristic gutters and folds and motor axons are myelinated and synapse elimination assures that only one axon is present at each NMS (reviewed in Sanes and Lichtman 2001).

## 3.3   NMS serves as a model system

The NMS is a very good model system in studying structural, functional and molecular aspects of a synapse. There are different reasons for that. First, as shown in figure 3.2, the NMS has a large size and is geometrically relative simple. Secondly, NMSs are readily accessible and NMSs are easy to see, partly because they are well separated from each other [Sanes & Lichtman, 2001]. Studies on the NMS can be performed *in vivo*, as well *in vitro*, due to the existence of muscle cell lines.

Additionally, the electric organ of *Torpedo californica* serves as a resource to isolate synaptic components in relatively large amounts [Cartaud et al., 2000] and $\alpha$-bungarotoxin (BTX), a 74-amino-acid polypeptide, the main component present in the deadly venom

of *Bungaris multicinctus*, binds specifically and quasi-irreversibly to muscle and electric organ AChRs [Lee et al., 1967]. This provided an important tool in research, for example 125I-BTX was initially used to identify AChRs, agarose-BTX was used to purify AChRs, and rhodamine-BTX was used to localize AChRs and to track their movements. Understanding the molecular properties of the NMS should help researchers to develop drugs for severe diseases such as Myasthenia gravis, Lambert Eaton syndrome, congenital myasthenic syndromes and the large group of muscle dystrophies.

## 3.4 Agrin, MuSK and Lrp4 - the major players in synapse formation

MuSK and Lrp4 are two receptors involved in postsynaptic differentiation at developing and adult NMSs. The importance of MuSK and Lrp4 became obvious through mouse molecular genetics approaches. MuSK deficient mice lack any postsynaptic specializations at the nerve-muscle contact and die perinatally [DeChiara, 1996]. Lrp4-mutant mice die at birth with defects in both presynaptic and postsynaptic differentiation, including aberrant motor axon growth and branching, a lack of acetylcholine receptor and postsynaptic protein clustering, and a failure to express postsynaptic genes selectively by myofiber synaptic nuclei [Weatherbee et al., 2006]. Agrin, which is released by motor terminals and deposited in the synaptic basal lamina, is the third key player during NMS developing. Agrin-deficient mice do not form functional postsynaptic structures and also die immediately after birth due to respiratory failure [Gautam et al., 1996].

### 3.4.1 Agrin

McMahan and colleagues noticed that the extracellular matrix of the NMS was sufficient to instruct synapses to re-form after losing nerve stimulation [Sanes, 1978]. This indicated that a trophic factor stably incorporated into the synaptic basal lamina was sufficient to induce pre- and postsynaptic differentiation. This factor was named agrin from the Greek "'agrein"' meaning "'to assembly", named after its ability to aggregate AChRs. The protein agrin was purified using the synapse-rich electric organ of the pacific electric ray *Torpedo californica* [Nitkin, 1987]. The gene encodes a protein of more than 2000 amino acids with a predicted molecular mass of 225 kDa, which can be increased to 600 kDa due to extensive N- and O-linked glycosylation of the amino-terminus. At least three of the O-linked carbohydrate attachment sites function as docking sites for heparan sulphate glycosaminoglycan (HS-GAG) side chains and assign agrin to the family of heparin sulfate proteoglycans [Tsen et al., 1995]. Agrin contains multiple epi-
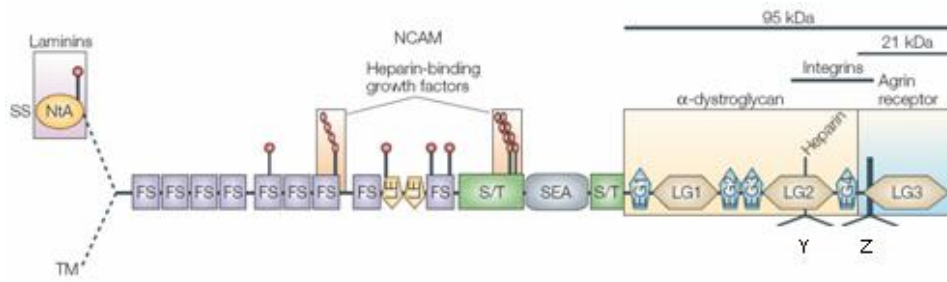
Figure 3.3: Structural domains of Agrin. LG, laminin globular domain; NCAM, neuronal cell adhesion molecule; S/T, serine/threonine-rich region; SEA, sea urchin sperm protein, enterokinase, agrin domain; (scheme published by Bezakova and Ruegg, 2003; modified).

dermal growth factor (EGF)-like signaling domains, two different laminin like domains, and multiple follistatin-like repeats (figure3.3). The four EGF-like domains and three laminin-like G domains are contained in the carboxy-terminal region, which is sufficient to induce AChR clusters in cultured myotubes; sequences in the amino-terminal region are thought to be responsible for the association of agrin with the extracellular matrix [McMahan, 1990, Tsen et al., 1995].

Amino-acid inserts at the Z site are crucial for agrin-induced AChR aggregation [Burgess et al., 1999]. On cultured myotubes, only the isoforms that contain an insert (called agrin-Z+) induce AChR aggregation and this activity is absent when the insert at the Z site is missing (called agrin-Z-) [Ruegg & Bixby, 1998]. The main source for the active agrin isoforms, those that can induce aggregation, is represented by neurons, including motor neurons. The signal sequence (SS) and amino (N)-terminal agrin domain (NtA) are present in an agrin isoform that is localized at the NMS. These two regions are responsible for the secretion of agrin (SS) and the binding to the basal lamina (NtA) [Bezakova & Ruegg, 2003].

## 3.4.2 MuSK

The Muscle-Specific Kinase (MuSK) is crucial for agrin triggered signaling at the NMS. Cultured myotubes devoid of MuSK do not aggregate AChR in response to agrin, and the ability of myotubes to aggregate AChR recovers after MuSK expression in restored [Herbst & Burden, 2000].

Agrin can activate MuSK in cultured myotubes, but not in myoblasts or other cells expressing MuSK [Glass et al., 1996], which implies that differentiated muscle cells contain another entity that functions as an 'agrin receptor'. This was identified as being Lrp4 (Low-density lipoprotein-receptor-related protein 4), that is also crucial for the formation of the NMS [Weatherbee et al., 2006]. It was shown that agrin can stimulate phosphorylation of MuSK in nonmuscle cells expressing Lrp4 and MuSK. The workgroup of Steven
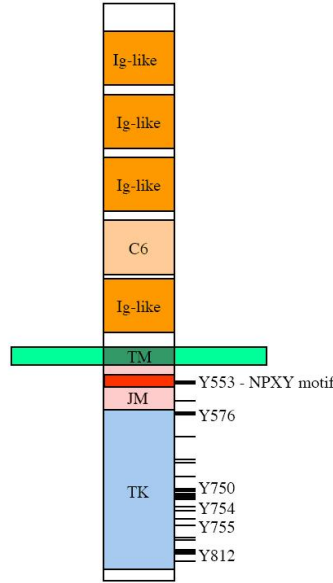
Figure 3.4: Schematic drawing of the MuSK protein. MuSK contains four immunglogulin-like (Ig) domains and one cysteine-rich (C6) domain in its extracellular portion which is separated from the intracellular part by a single transmembrane domain (TM). The cytosolic domain can be divided into a juxtamembrane (JM) domain and a kinase domain (TK). Tyrosines in these two domains become phosphorylated in response to agrin. Tyrosine 553, which lies within an NPXY motif in the JM domain has been shown to be essential for AChR clustering.

Burden determined that Lrp4 is sufficient to reconstitute agrin-stimulated MuSK phosphorylation in BaF3 cells that expressed MuSK and Lrp4 [Kim et al., 2008], and the workgroup of Lin Mei showed that Lrp4 expression enables MuSK activation by agrin in HEK293 cells [Zhang et al., 2008].

As shown in figure 3.4, MuSK is a transmembrane receptor, with a cytoplasmatic, extracellular and transmembrane domain. The cytoplasmatic domain, contains the tyrosine kinase domain and shows similarities with neurotrophin receptors. The extracellular domain contains four immunoglobulin-like domains and a cysteine-rich domain. The MuSK intracellular domain contains a juxtamembrane domain, a kinase domain and an eight amino acid carboxy-terminal tail [Valenzuela et al., 1995].

The cytoplasmic domain of MuSK contains 17 tyrosine residues within the kinase domain and one tyrosine residue in the juxtamembrane region [Valenzuela et al., 1995]. Only 6 of these tyrosine residues (shown in figure 3.4) are accessible for phosphorylation [Watty et al., 2000]. It was shown that the juxtamembrane tyrosine residue Y553 is essential for downstream signaling, since myotubes expressing MuSK Y553F fail to cluster AChRs in response to agrin. MuSK Y553 is further required to stimulate AChR $\beta$-subunit tyrosine phosphorylation, which precedes, but is not required for AChR clustering. This

suggests that MuSK activates or recruits a kinase that has a role in catalyzing tyrosine phosphorylation of AChRs and stimulating AChR clustering [Herbst & Burden, 2000]. More than that, Y553 is located within an NPXY motif, which can function as an internalization signal in other membrane receptors [Chen et al., 1990] and, when phosphorylated serves as a binding motif for proteins containing phosphotyrosine-binding (PTB) domains [Blaikie et al., 1994, Kavanaugh & Williams, 1994]. This finding supports the idea, that phosphorylated tyrosines act as docking sites for molecules that pass on the signal elicited by agrin [Herbst & Burden, 2000].

### 3.4.3 Agrin signal transduction events at the neuromuscular synapse

Agrin initiates signal transduction events starting with MuSK activation [Jennings & Burden, 1993, Glass et al., 1996]. This requires its agrin co-receptor Lrp4 [Kim et al., 2008, Zhang et al., 2008]. After its activation, MuSK signals via the proteins called Casein kinase 2 (CK2) [Cheusova et al., 2006], Dok-7 [Okada et al., 2006] and rapsyn, to induce "clustering" of acetylcholine receptors (AChR). Both CK2 and Dok-7 are required for MuSK induced formation of the neuromuscular junction, since mice lacking Dok-7 failed to form AChR clusters or neuromuscular synapses, and since downregulation of CK2 also impedes recruitment of AChR to the primary MuSK scaffold.

MuSK phosphorylation and subsequent activation of several intracellular enzymes are necessary for agrin-induced AChR aggregation. Among this enzymes, are tyrosine kinases such as Abl and Src-family members [Finn et al., 2003, Sadasivam et al., 2005], geranylgeranyltransferase I, a metalloenzyme involved in protein prenylation [Luo et al., 2003], the serine kinase casein kinase 2 [Cheusova et al., 2006], small GTPases of the Rho family [Luo et al., 2002], and p21-activated kinase (PAK) / Dishevelled (Dvl) [Luo et al., 2003]. *In vitro* studies indicate a necessary role of these enzymes for agrin-induced AChR aggregation

Taken together, at the NMS, receptors such as MuSK, ErbBs, integrins might activate distinct signaling pathways that tailor cytoskeletal architecture, allow the integration of diverse signals and activate the transcription of synapse-specific genes [Sadasivam et al., 2005]. A schematic drawing of agrin-induced signaling events at the NMS is shown in figure 3.5.
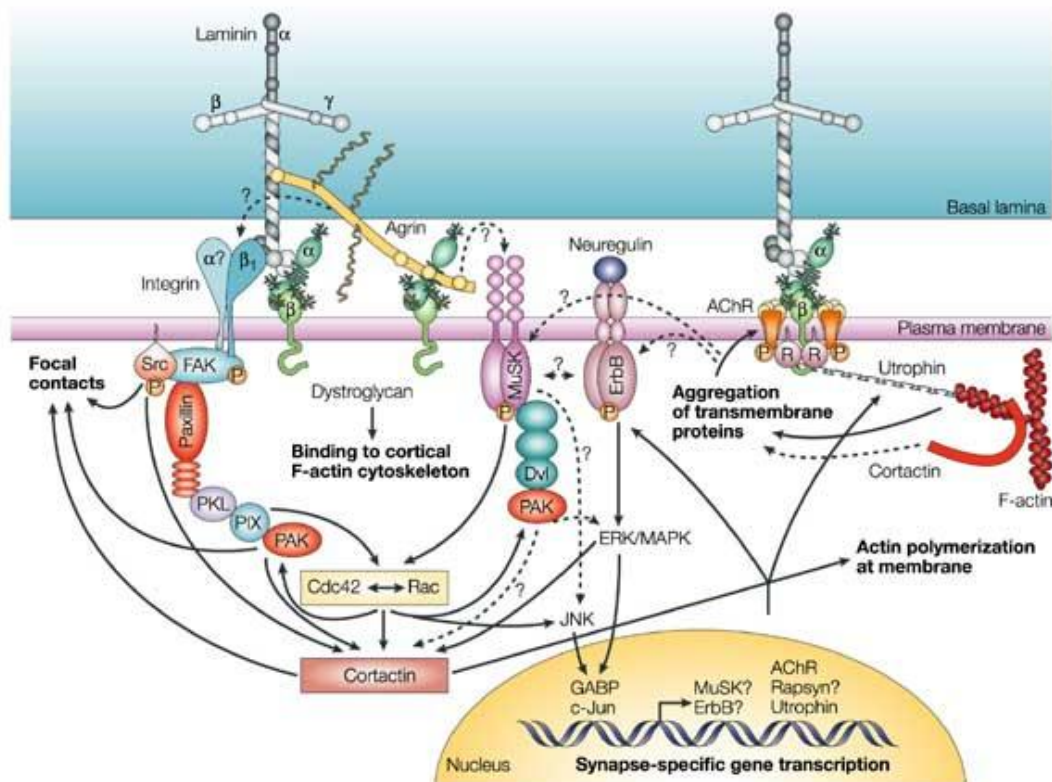
Nature Reviews | Molecular Cell Biology

Figure 3.5: Signaling activated by agrin-B/z+ at the NMS. At the NMS, agrin activates MuSK and other receptors and this leads to the aggregation of acetylcholine receptors (AChRs). Integrins engaged by agrin directly or indirectly (through binding to laminin) might participate in cytoskeletal re-organization through focal adhesion kinase (FAK) and Src. Activated MuSK, ErbB receptors and integrins might in turn activate transcription factors such as c-jun and GABP to initiate synaptic transcription. The newly synthesized proteins, such as AChR, rapsyn (R) and utrophin might further stabilize the postsynapse by connecting it to the cytoskeleton. Formation and maintenance of a mature postsynapse involves 'crosstalk' between distinct pathways. Cortactin might function as a checkpoint for several pathways involved in the cytoskeleton rearrangement. Dystroglycan stabilizes the mature synapse by connecting the basal lamina to the cortical F-actin cytoskeleton. Integrins might also contribute to the stability of the NMS by regulating the turnover of focal contacts through Src and PAK. PAK is recruited to integrin through a paxillin scaffold. Dotted arrows with question marks indicate hypothetical interactions. The requirement of GABP and c-jun for MuSK, ErbB and rapsyn transcription has not been investigated. GABP, guanidine and adenosine-binding protein; PIK, PAK-interacting exchange factor; PKL, paxillin kinase linker (published by Bezakova and Ruegg, 2003).

20

Nature Reviews | Molecular Cell Biology
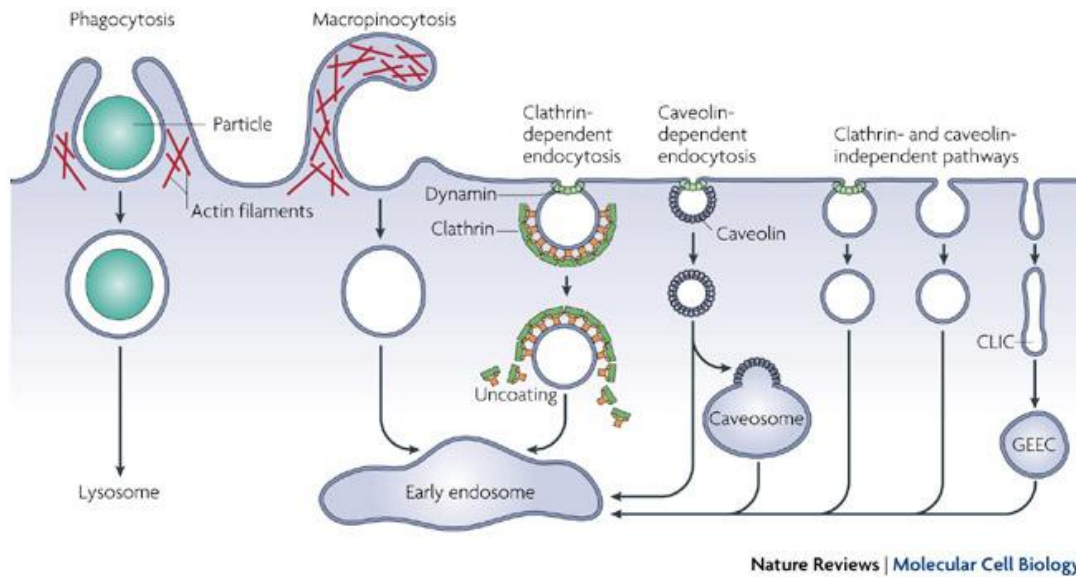
Figure 3.6: Pathways of entry into cells. Large particles can be taken up by phagocytosis, whereas fluid uptake occurs by macropinocytosis. Numerous cargoes can be endocytosed by mechanisms that are clathrin and dynamin dependent, caveolin and dynamin dependent or clathrin and caveolin independent. Most internalized cargoes are delivered to the early endosome via vesicular (clathrin- or caveolin-coated vesicles) or tubular intermediates (known as clathrin- and dynamin-independent carriers (CLICs)) that are derived from the plasma membrane. Some pathways may first traffic to intermediate compartments, such as the caveosome or glycosyl phosphatidylinositol-anchored protein enriched early endosomal compartments (GEEC), en route to the early endosome (published by Mayor and Pagano, 2007).

## 3.5 Endocytosis and signaling

### 3.5.1 Short classification of endocytosis

There are numerous ways that endocytic cargo molecules may be internalized from the surface of eukaryotic cells. A short classification is shown in figure 3.6. Any endocytic pathway that mediates the transport of a specific cargo will first require mechanisms for selection at the cell surface. Next, the plasma membrane must be induced to bud and pinch off. Finally, mechanisms are required for tethering these vesicles to the next stop on their itinerary and for inducing their subsequent fusion to this target membrane [Mayor & Pagano, 2007].

In this study I focused my attention on dynamin dependent endocytosis to better characterize MuSK internalization and its influence on agrin induced signaling at the NMS. Shown in figure 3.7, are different types of endocytosis that are dynamin dependent. Dynamin was originally noted for its role in severing clathrin-coated vesicles from the plasma membrane and was subsequently found to be involved in a clathrin-independent

21
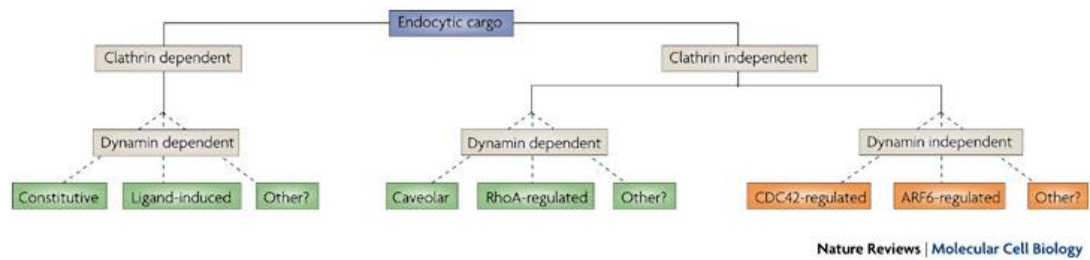
Figure 3.7: Dynamin involvement in different endocytic mechanisms. A cargo protein can be endocytosed by either clathrin-dependent or clathrin-independent (CI) mechanisms. The CI pathways can be further categorized first by their dependence on the large GTPase dynamin, and then by other mechanistic components of the internalization pathway (published by Mayor and Pagano, 2007).

(CI) pathway that is mediated by caveolae. Because vesicle scission at the plasma membrane is required for subsequent internalization, it was initially assumed that dynamin might have a role in all forms of endocytosis. However, it was later discovered that some CI pathways are dynamin-independent, at least when they are assessed by monitoring cargo internalization in the context of exogenous expression of mutant dynamin isoforms [Damke, 1995] or from analysis of organisms that are homozygous for mutant dynamin [Guha et al., 2003].

## 3.5.2 Dynamin and dynasore influence on endocytosis

Dynamin, a 100-kDa GTPase, is an essential component of vesicle formation in receptor-mediated endocytosis, synaptic vesicle recycling, caveolae internalization, and possibly vesicle trafficking in and out of the Golgi. In addition to the GTPase domain, dynamin also contains a pleckstrin homology domain (PH) implicated in membrane binding, a GTPase effector domain (GED) shown to be essential for self-assembly and stimulated GTPase activity, and a C-terminal proline-rich domain (PRD), which contains several SH3-binding sites (figure 3.8). Dynamin interaction partners bind to the PRD and may either stimulate GTPase activity or target dynamin to the plasma membrane. Purified dynamin readily self-assembles into rings or spirals. This striking structural property supports the hypothesis that dynamin wraps around the necks of budding vesicles where it plays a key role in membrane fission [Hinshaw, 2000].

Although only one dynamin isoform has been identified in *Drosophila* and *Caenorhabditis elegans* [Chen et al., 1991], in mammals three closely related isoforms have been identified, for review see [Urrutia et al., 1997]. Dynamin 1, found specifically in neuronal tissue [Scaife, 1990], has 8 splice variants [Bonifacino et al., 1998] and has been mapped
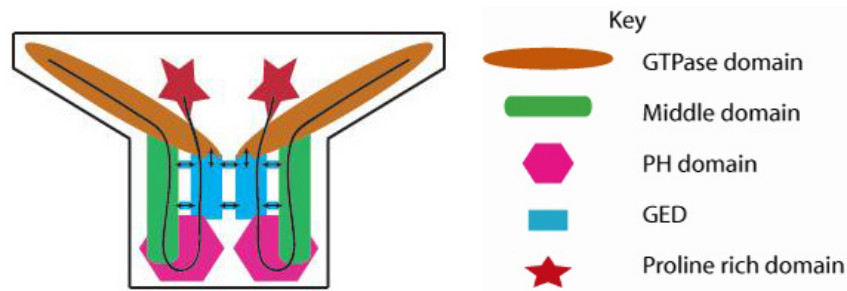
Figure 3.8: Diagram of dynamin dimer domain structure where the small arrows indicate intra-molecular interactions between domains. GED is GTPase effector domain, (picture from http://www.endocytosis.org/Dynamin/Middle-GED.html).

to human chromosome 9q34 [Newman-Smith et al., 1997]. Dynamin 2 is ubiquitously expressed [Cook et al., 1994] and has 4 splice variants [Bonifacino et al., 1998], whereas dynamin 3, expressed predominantly in testes [Nakata, 1993], but also found in lung and neurons [Cook et al., 1996], has 13 splice variants [Bonifacino et al., 1998]. It was schown that different dynamin isoforms play overlapping roles in different types of endocytosis. For example, it was shown that dynamin 1 and dynamin 2 simultaneously participate in the clathrin-independent and -dependent membrane retrieval in pancreatic beta cells [Lu et al., 2008].

Dynamin 2 dominant negative mutant (dyn2-K44A) more potently inhibited receptor-mediated endocytosis than dyn1-K44A in HeLa cells and at the basolateral surface of polarized MDCK cells. In contrast, dyn1(K44A) more potently inhibited endocytosis at the apical surface of MDCK cells [Altschuler et al., 1998].

Another important discovery in studying dynamin dependent endocytosis was "'dynasore"'. Macia and colleagues [Macia et al., 2006] have discovered "'dynasore"' in their search through approximately 16,000 small molecules to identify a chemical inhibitor for dynamin. Dynasore functions as an inhibitor of dynamin 1 and dynamin 2 GTPase activity and blocks endocytic functions previously shown to require dynamin. Previously methods such as siRNA and expression of dominant-negative dynamin have been used to test dynamin-mediated processes. These methods are slow acting and could produce secondary effects [Thompson & McNiven, a]. Dynasore acts fast and reversible, is cell permeable and offers a direct and precise tool in blocking dynamin dependent endocytosis.

### 3.5.3 Endocytosis and signaling of receptor tyrosine kinase

Endocytosis of receptor tyrosine kinases (RTKs) has been shown to be necessary for intracellular signaling in response to various growth factors. The internalization of

activated receptors leads to either attenuation of signaling via degradation of the ligand/receptor complex or reduction of signaling from endosomes [Ceresa & Schmid, 2000, Wang et al., 2004]. The induction of the appropiate biological outcome requires signaling of the correct magnitude, kinetics and specificity [Marmor & Yarden, 2004, Marshall, 1995]. Thus, signaling through RTKs must be subject to tight regulation. The epidermal growth factor receptor (EGFR) has served as a paradigm for the elucidation of RTK-induced signaling pathways. It was shown that ligand-induced receptor endocytosis is required for signal transduction by the EGF receptor [Vieira et al., 1996, Brugge et al., 2001]. But most importantly, it was shown that neuregulin-mediated endocytosis of ErbB receptor tyrosine kinase is important for subsequent Erk activation which is required for AChR expression [Yang et al., 2005]. In addition, it was shown that the internalization requires the kinase activity of ErbB and involves a clathrin-dependent endocytic pathway. These findings demonstrate that receptor trafficking and signaling are closely linked. In the muscle, endosomal compartments are highly concentrated beneath the NMSs and endocytosis is considered to be of particular importance in the control of postsynaptic receptor density [Salpeter et al., 1993, Xu & Salpeter, 1997]. Furthermore, increasing evidence implicate trafficking of synaptic proteins as crucial events during NMS formation and maintenance. How localization and interacting proteins impact protein function and influence signaling is an important theme, as is the potential for modulating signaling through therapeutic targeting of activated receptors and components of the endocytic machinery [Mukherjee et al., 2006].

Until now evidence has been provided, that inhibition of MuSK endocytosis attenuates agrin-induced AChR clustering [Zhu et al., 2008]. The researchers could show that expression of a dominant-negative mutant of dynamin in muscle cells, reduces MuSK internalization and agrin-MuSK signaling. As a result, AChR clustering is also reduced. In addition it was shown that MuSK undergoes ligand-mediated endocytosis, just like other receptor tyrosine kinases such as EGFR and ErbB4 [Zhu et al., 2008].

### 3.5.4 Tagging receptors and following their internalization

An useful tool in following receptors internalization is to specifically label them with fluorophores. McCann and collegues [McCann et al., 2005] developed a method where they generated fusion proteins that incorporate short sequences recognized by streptavidin (SA). SA is an ideal marker of transmembrane molecules because SA exhibits little nonspecific binding, does not cross the cell membrane, accesses more sterically restricted spaces than antibodies, does not interfere with protein localization or function due to its small size and is more reliable than antibodies that are very large and thus can interfere with endocytosis processes. The best available SA-binding sequence, called SBP-Tag

[Keefe et al., 2001] is a 38-mer that recognizes the biotin binding site of SA. Thus, the receptor of interest is tagged with SBP-Tag, pulse-labeled with different streptavidin conjugates and its internalization visualized with a fluorescent microscope.

## 3.6   Aim of my project

Studies on RTKs have shown that endocytosis and trafficking of cell surface receptors can modulate signaling pathways. The aim of this study is to characterize MuSK endocytosis for a better understanding of its function in MuSK signaling. According to this theme, my work had two main research aims. The first one was to ellucidate the role of dynamin in MuSK endocytosis. Different questions had to be answered for this purpose, questions like: is MuSK endocytosis dynamin dependent? What dynamin isoform is responsible for MuSK endocytosis? Does perturbation of MuSK endocytosis using a dynamin dominant-negative mutant or dynasore (a dynamin inhibitor) have an influence on agrin-induced AChRs clustering in muscle cells? Another aim of my research was to generate a muscle cell line expressing SBP-tagged MuSK, that can specifically be stained with different fluorophores and its internalization be followed. This allowed me to visualise colocalisations of MuSK with different compartments of the endocytic pathway (early endosomes). The results of this study are described in the next chapter.

# Chapter 4

# Results

## 4.1 Influence of dynamin on MuSK endocytosis and signaling

The effect of dynamin on MuSK endocytosis was studied in transfected HeLa cells where MuSK-SBP was specifically labeled with fluorescently labeled streptavidin and its endocytosis visualised with a fluorescence microscope. As shown in figure 4.1, the SBP-Tag (SBP= streptavidin binding protein), is recognized by the biotin binding site of StreptAvidin (SA). Different fluorophore conjugates of SA can be used for staining the cells [McCann et al., 2005]. This allows us to specifically stain MuSK-SBP receptors and follow their trafficking in transfected HeLa cells.

In order to see the influence of dynamin on MuSK-SBP endocytosis, HeLa cells were cotransfected with a dominant-negative mutant of dynamin (dyn-K44A) or with dynamin wild-type (dyn-WT) and MuSK-SBP. Surface MuSK-SBP receptors were specif-
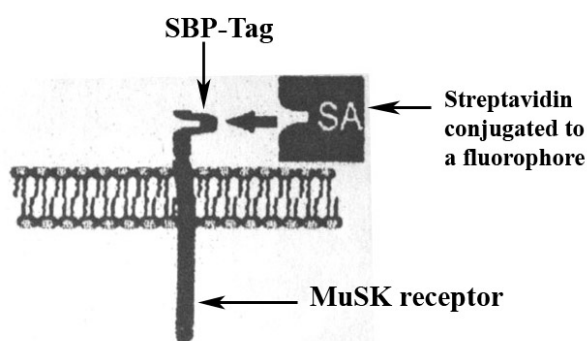


Figure 4.1: MuSK receptor expressing the SBP-Tag. SA-StreptAvidin. SBP-StreptAvidin Binding Protein.
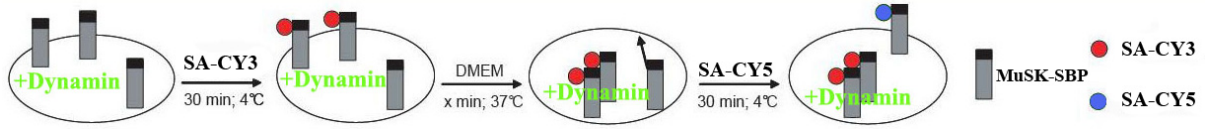
Figure 4.2: Scheme representing experimental approach to check the effect of dynamin on MuSK-SBP endocytosis in HeLa cells. HeLa cells are first cotansfected with MuSK-SBP and dyn-K44A or dyn-WT. Cells are stained at 4°C with SA-Cy3 (Streptavidin-Cy3), incubated for x minutes in DMEM medium at 37°C and then stained again at 4°C with SA-Cy5 (Streptavidin-Cy5).

ically stained at 4°C with Streptavidin-Cy3 (SA-Cy3) or with Streptavidin-Alexa 594 (SA-Alexa 594), both represented in figures in red color. Afterwards, HeLa cells were incubated at 37°C when endocytosis occurs, for different time intervals. In some experiments, surface MuSK-SBP was subsequently stained at 4°C with Streptavidin-Cy5 (SA-Cy5) represented in figures in blue (figure 4.2). Cells were fixed in 4% PFA, mounted in Vectashield medium and visualised with a fluorescence microscope.

### 4.1.1 Dynamin 1 and its influence on MuSK endocytosis in HeLa cells

As a control experiment, a time course of MuSK-SBP endocytosis in HeLa cells was performed (figure 4.3). Cells were transfected only with MuSK-SBP and stained at 4°C with SA-Cy3 (red). Cells were incubated at 37°C for different time intervals, when endocytosis occurs and surface MuSK-SBP was stained at 4°C with SA-Alexa 488 (green). At time point 0 cells were stained only at 4°C with both fluorophores. A strong colocalisation of surface MuSK-SBP receptors can be seen, represented by the yellow dots. For the other time intervals we can see an accumulation of MuSK-SBP inside the cells (red staining), representing endocytosis of the MuSK protein.

In order to study the effect of dynamin 1 on MuSK-SBP endocytosis, HeLa cells were cotransfected with dyn1-K44A-GFP and MuSK-SBP. Cells were stained at 4°C with SA-Alexa 594 (red). Cells were incubated at 37°C when endocytosis occurs, for different time intervals. Subsequently cells were fixed and examined with a fluorescence microscope as described in Materials and methods. As shown in figure 4.4, the dominant-negative mutant of dynamin 1 did not inhibit MuSK-SBP endocytosis in HeLa cells. After 30 minutes incubation at 37°C, MuSK-SBP clusters can be seen and after 2 hours MuSK-SBP is internalised. As a primary conclusion of this experiment, dynmain 1 is not involved in MuSK endocytosis in transfected HeLa cells because expression of dyn1-K44A does not inhibit MuSK-SBP endocytosis.
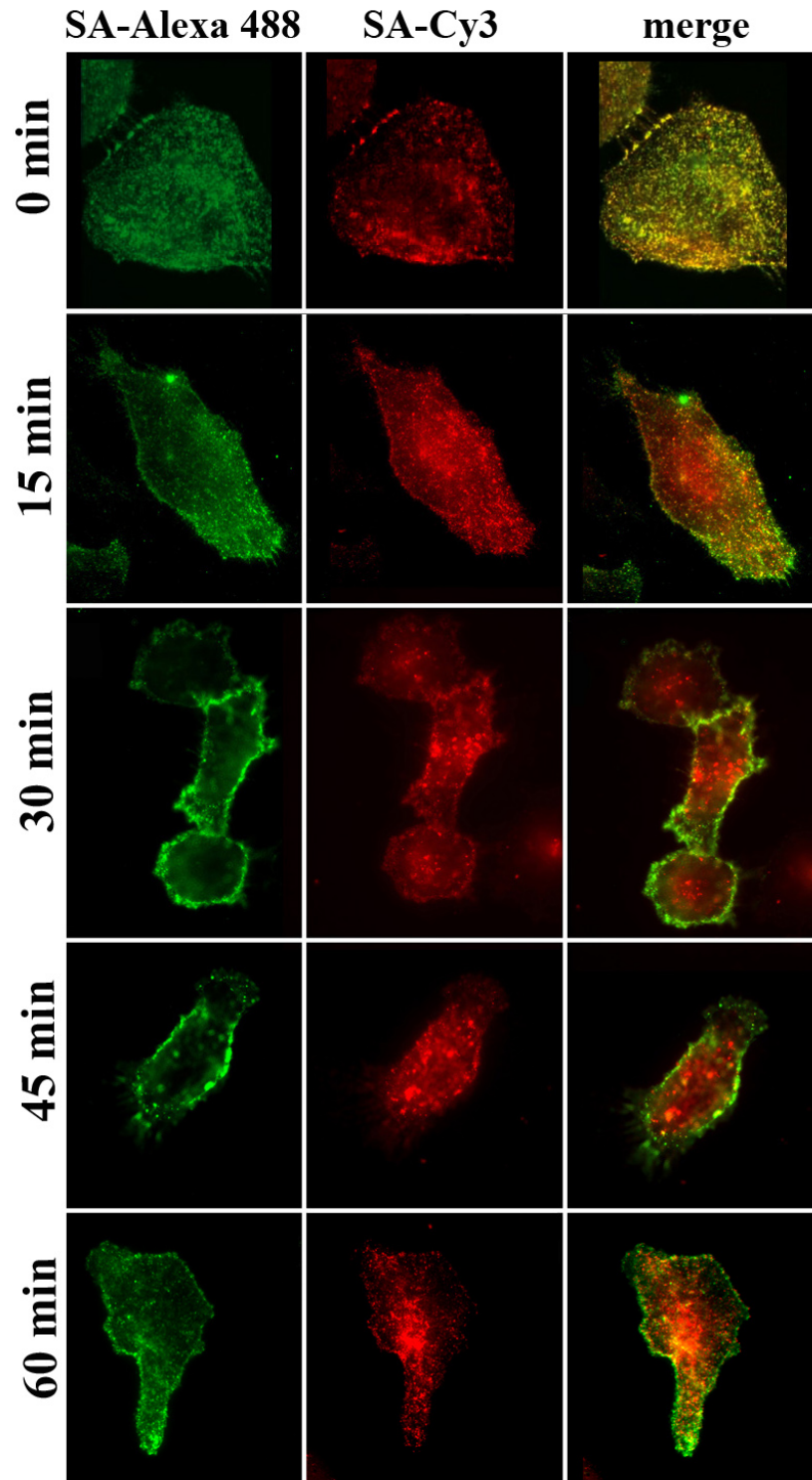
Figure 4.3: Time course of MuSK-SBP endocytosis in transfected HeLa cells. In the middle panel MuSK-SBP stained with SA-Cy3 (red) was incubated for different time intervals: 0, 30, 60, 120 and 240 minutes. In the left panel surface MuSK-SBP was stained with SA-Alexa 488 (green), after endocytosis took place. The right panel represents a merge between SA-Cy3 and SA-Alexa 488.
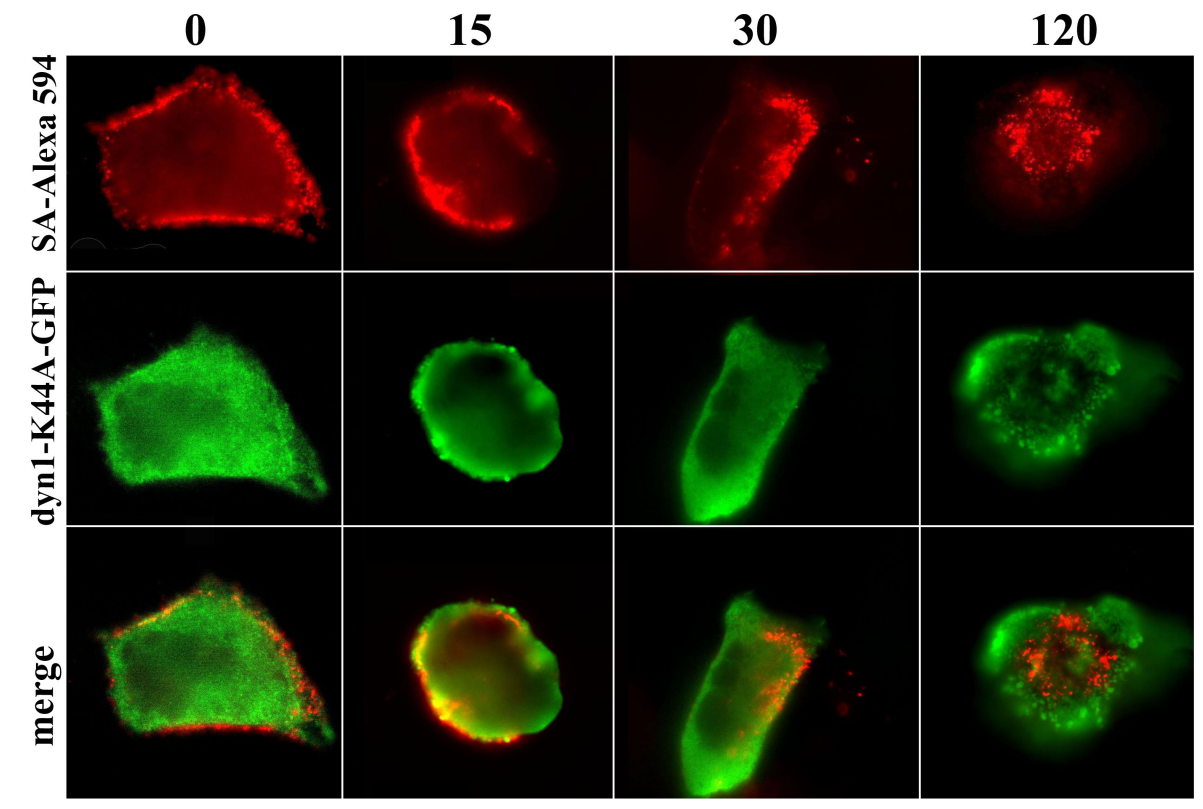
Figure 4.4: The effect of dynamin 1 on MuSK-SBP endocytosis in HeLa cells. HeLa cells were transfected with dyn1-K44A-GFP and MuSK-SBP. In the top panel MuSK-SBP is stained with SA-Alexa 594 (red) and incubated for different time intervals: 0, 15, 30 and 120 minutes at 37°C. In the middle panel HeLa cells expressing dyn1-K44A-GFP are shown. The bottom panel represents a merge between the first two panels. MuSK internalization proceeds with increasing time intervals.

### 4.1.2 Dynamin 2 and its influence on MuSK endocytosis in HeLa cells

HeLa cells were cotransfected with a dynamin 2 dominant-negative mutant (dyn2-K44A-GFP) or with dynamin 2 wildtype (dyn2-WT) and MuSK-SBP. Cells were stained at 4°C with SA-Cy3 (red). Cells were incubated for 15 minutes at 37°C when endocytosis occurs. Surface MuSK-SBP was subsequently stained at 4°C with SA-Cy5 (blue). Cells were fixed and examined with a fluorescence microscope as described in Materials and methods. As shown in figure 4.5, after 15 minutes incubation, cells transfected only with MuSK-SBP, have intracellular clusters of MuSK-SBP. On the other hand, in the cells transfected with dyn2-K44A, MuSK-SBP internalization was greatly delayed, and a significant colocalisation is visible between MuSK incubated at 37°C and surface MuSK (magenta color). Cells transfected with dyn2-WT, had an increase in MuSK internalization compared with the control cells. MuSK-SBP clusters are detectable in the middle of the cell. As a conclusion, dynamin 2 seems to play a role during MuSK endocytosis.

Subsequently, I performed a time course for MuSK endocytosis in HeLa cells expressing dyn2-K44A. Cells were first transfected with dyn2-K44A and MuSK-SBP and then surface MuSK-SBP was stained at 4°C with SA-Cy3. Cells were incubated at 37°C for different time intervals and afterwards surface MuSK-SBP was stained at 4°C with SA-Cy5. Cells were fixed and visualised with a fluorescence microscope. MuSK-SBP stained with SA-Cy3 (red) and incubated for 15, 30 and 60 minutes, colocalises with surface MuSK-SBP stained with SA-Cy5 (blue), during this time points (figure 4.6). Internal MuSK clusters are barely visible indicating that dynamin 2 affects MuSK endocytosis in HeLa cells by regulating surface MuSK internalization.

### 4.1.3 Influence of MuSK kinase activity on dynamin 2 mediated endocytosis in HeLa cells

Ligand-induced stimulation of RTKs often results in an increased endocytosis of the active receptor. Since MuSK can not be stimulated with agrin in non-muscle cells, expression of a constitutive-active MuSK protein represents an alternative to study the effect of kinase activity on MuSK endocytosis. Over-expression of a constitutively-active MuSK mutant (MuSK LS745/746MT) in COS cells confirmed that the kinase-domain is active without agrin stimulation (Susan Luiskandl, unpublished data).

In this experiment I determined whether endocytosis of constitutively-active MuSK in HeLa cells is also reduced upon expression of dyn 2-K44A. For this purpose a MuSK-SBP-KA(constitutively-active) construct was produced. HeLa cells were cotransfected with dyn2-K44A and MuSK-SBP-KA. As a control, cells were transfected only with
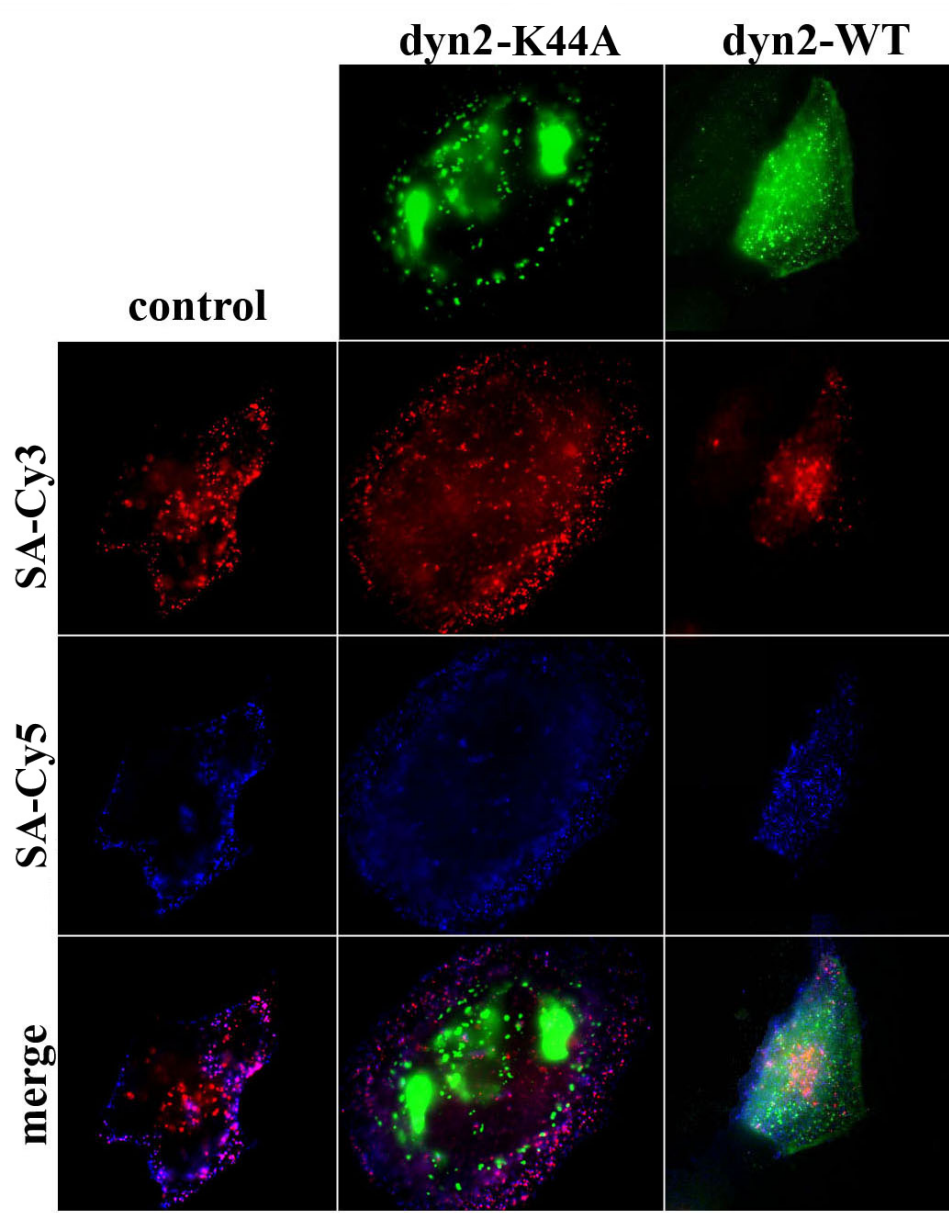
Figure 4.5: Influence of dyn2-K44A and dyn 2-WT on MuSK-SBP endocytosis in transfected HeLa cells. The left panel represents a control where HeLa cells were transfected only with MuSK-SBP. The middle vertical panel represents HeLa cells transfected with dyn2-K44A/MuSK-SBP and the right vertical panel represents HeLa cells transfected with dyn2-WT/MuSK-SBP. The top panel shows HeLa cells transfected with dyn2-K44A-GFP and dyn2-WT-GFP, the second panel represents MuSK-SBP stained with SA-Cy3 (red) and incubated for 15 minutes at 37°C. The third panel panel represents surface MuSK stained with SA-Cy5 (blue) and the bottom panel is a merge between all panels. The colocalisation between MuSK-SBP stained with SA-Cy3 (red) and surface MuSK-SBP stained with SA-Cy5 (blue) is represented in magenta color.
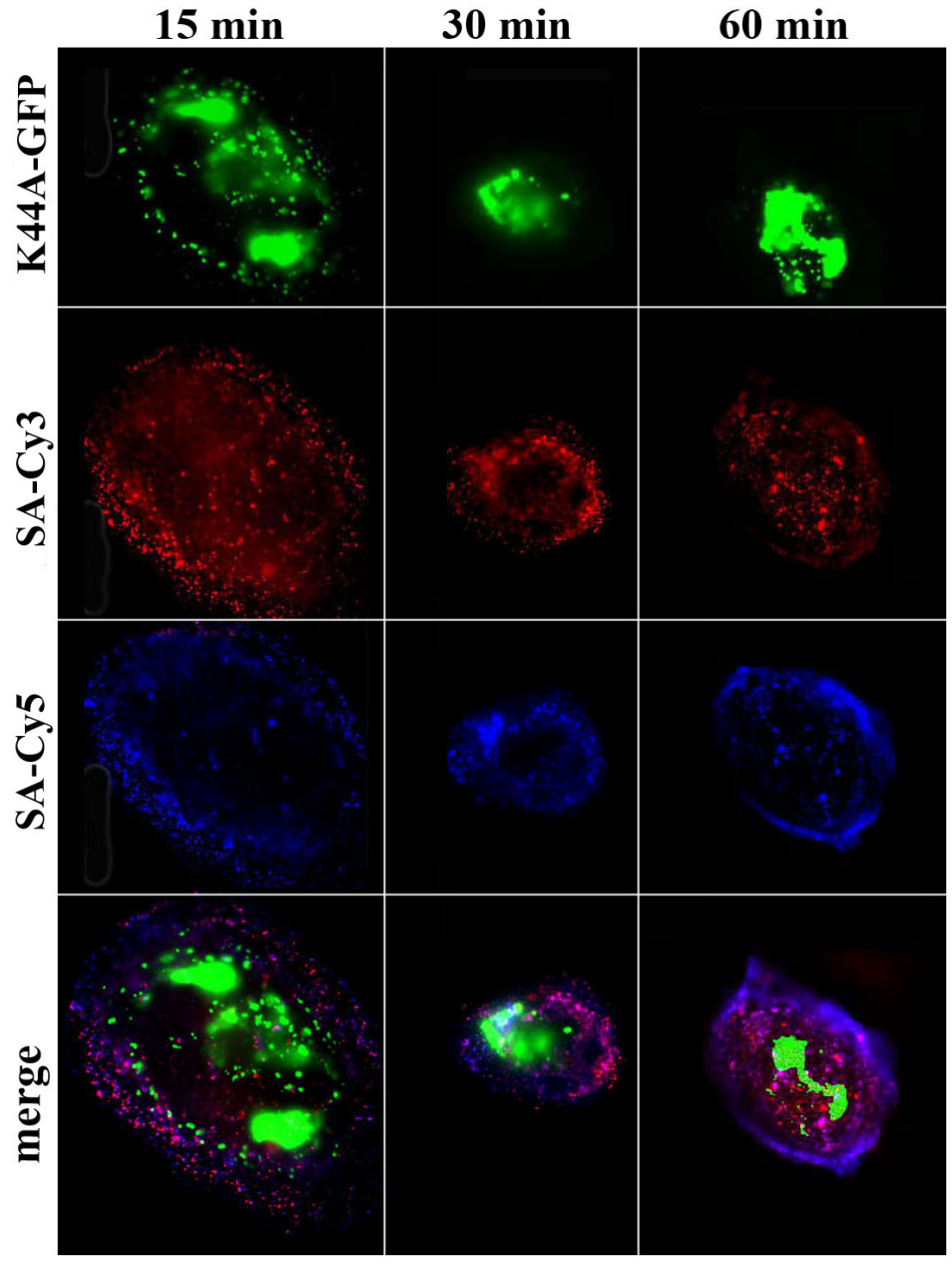
Figure 4.6: Influence of dynamin 2 on MuSK-SBP endocytosis in HeLa cells within different periods of time. HeLa cells transfected with dyn2-K44A and MuSK-SBP were stained at 4°C with SA-Cy3 and incubated for 15, 30 and 60 minutes at 37°C. Subsequently surface MuSK-SBP was stained at 4°C with SA-Cy5. The top panel represents HeLa cells transfected with dyn2-K44A-GFP (green),the second horizontal panel represents MuSK-SBP stained with SA-Cy3 (red)and incubated for 15, 30 and 60 minutes at 37°C. The third horizontal panel represents surface MuSK-SBP stained with SA-Cy5 (blue). The bottom horizontal panel is a merge between the first 3 lanes. Magenta color represents the colocalisation between MuSK-SBP stained with SA-Cy3 (red) and incubated for different time intervals and surface MuSK-SBP stained with SA-Cy5 (blue).

| K44A-GFP | SA-Cy3 | SA-Cy5 | merge | control/merge |
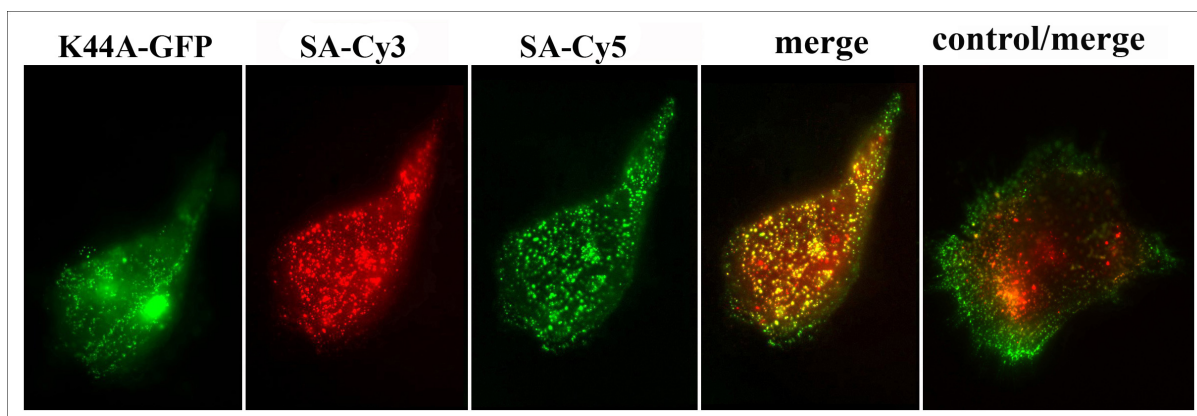
Figure 4.7: Influence of MuSK kinase activity on dynamin 2 mediated MuSK endocytosis. HeLa cells were cotransfected with dyn2-K44A and MuSK-SBP-KA (kinase active) or only with MuSK-SBP-KA in control experiment. Surface MuSK was stained at 4°C with SA-Cy3, cells were incubated at 37°C for 45 minutes, and surface MuSK was stained with SA-Cy5. The left panel shows HeLa cells, expressing dyn2-K44A-GFP. The second panel represents MuSK-SBP-KA stained with SA-Cy3 (red), third panel represents surface MuSK-SBP-KA stained with SA-Cy5 (artificial colored in green in the image), fourth panel represents a merge between the previously two panels. The colocalisation between SA-Cy3 (red) and SA-Cy5 (green) is represented in yellow color. The last lane represents the control, in red is MuSK-SBP-KA stained with SA-Cy3,incubated for 45 minutes, and in green is surface MuSK-SBP-KA stained with SA-Cy5 (artificially colored in green). SA-Cy5 is shown in green since the overlap of red and green, (yellow) is visually better perceived compared with magenta, the overlap of red and blue.

MuSK-SBP-KA. Cells were stained at 4°C with SA-Cy3 (red), incubated for 45 minutes at 37°C, and then surface MuSK-SBP-KA was stained at 4°C with SA-Cy5. Figure 4.7 shows that MuSK-SBP-KA was internalized when transfected alone, but when cotransfeced with dyn2-K44A, its endocytosis was inhibited. Numerous yellow dots representing colocalisations between internalised MuSK-SBP-KA and surface MuSK-SBP-KA are visible.

## 4.1.4 Influence of dynasore on MuSK endocytosis in HeLa cells

Dynasore, a cell-permeable small molecule was discovered by Macia et al. as an inhibitor of dynamin endocytic functions [Macia et al., 2006]. Dynasore inhibits all dynamin isoforms involved in endocytosis. It acts fast and provides an useful tool in studying endocytic and dynamin-dependent mechanisms. In this experiment HeLa cells were transfected with MuSK-SBP. I first performed a starvation, where cells were kept in DMEM medium for 30 minutes. Afterwards a preincubation with dynasore was performed (the inhibitor was added to cells medium for 30 minutes). This time period was shown in different publications as sufficient for dynasore to act and block dynamin dependent

endocytosis. As a control, DMSO was added to the medium (because dynasore was dissolved in DMSO). Cells were washed in cold PBS and MuSK-SBP was stained at 4°C with SA-Cy3. Cells were incubated in medium with dynasore or DMSO at 37°C for 45 minutes to let endocytosis occur. After 45 minutes, cells were washed in cold PBS and surface MuSK-SBP was stained at 4°C with SA-Alexa488. Cells were fixed in 4% PFA and mounted in Vectashield medium. Cells were visualised with a fluorescence microscope. In cells treated with dynasore, MuSK-SBP endocytosis was inhibited (figure 4.8). A strong colocalisation between MuSK-SBP stained with SA-Cy3 and surface MuSK-SBP stained with SA-Alexa488 is observed demonstrating an effect on MuSK endocytosis. On the other hand, in control experiment, where cells were not preincubated with dynasore, big red clusters of MuSK-SBP stained with SA-Cy3 can be observed inside the cell and little colocalisation with surface MuSK-SBP stained with SA-Alexa488 is visible. Thus, blocking dynamins, we interfere with MuSK-SBP internalization in transfected HeLa cells.

## 4.1.5 Influence of dynasore on agrin induced AChR clustering in muscle cells

To test whether inhibition of dynamin-dependent endocytosis has an effect on MuSK signaling, agrin-induced AChR clustering was studied in the presence of dynasore.
C2C12 myoblasts were switched to differentiation medium to induce myotubes formation. Myotubes were preincubated for 30 minutes with dynasore, DMSO, or left in DM (differentiation medium). Subsequently, agrin was added to the medium to induce AChR cluster formation for 8 hours. Cells were fixed in 4% PFA and AChRs were stained with $\alpha$-BGT-Alexa 594 and sampels were visualised with a fluorescence microscope. Number and length of AChRs clusters were quantified from at least 10 fields visualized with a 63X obiective. As shown in figure 4.9 dynasore interferes with AChR clustering. Agrin-induced AChR clusters in myotubes treated with dynasore are smaller and their number is incresed.

## 4.1.6 Influence of dynasore on AChR phosphorylation after agrin stimulation

Stimulation of muscle cells with agrin leads to AChR clustering. In addition, the agrin/MuSK signaling pathway involves tyrosine phosphorylation of the AChR$\beta$ subunit. Since the previous experiment revealed an effect of dynasore on AChR clustering, I tested whether dynasore affects AChR $\beta$ tyrosine phosphorylation. C2C12 myotubes were first incubated in medium with dynasore, DMSO or left in DMEM for 30 minutes. Agrin was added
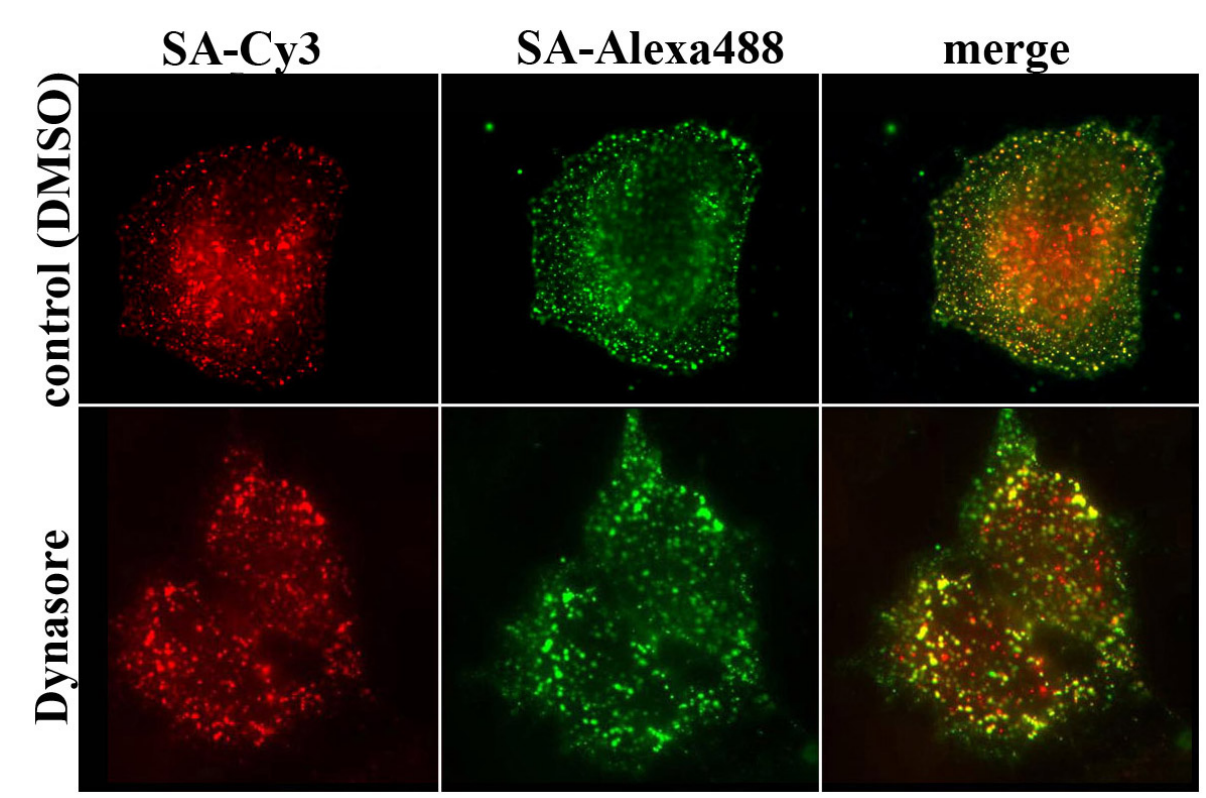
Figure 4.8: Influence of dynasore on MuSK-SBP endocytosis in HeLa cells. MuSK-SBP transfected cells were preincubated with dynasore or with DMSO (control). Surface MuSK-SBP was stained at 4°C with SA-Cy3 (red) and cells were subsequently incubated at 37°C for 45 minutes. Afterwards, surface MuSK-SBP was stained at 4°C with SA-Alexa488 (green). First vertical panel from right, represents MuSK-SBP stained with SA-Cy3 (red), middle vertical panel represents surface MuSK-SBP stained with SA-Alexa488 (green) and the left vertical panel represents a merge between SA-Cy3 and SA-Alexa488. Yellow dots represent the colocalisation between SA-Cy3 and SA-Alexa488.
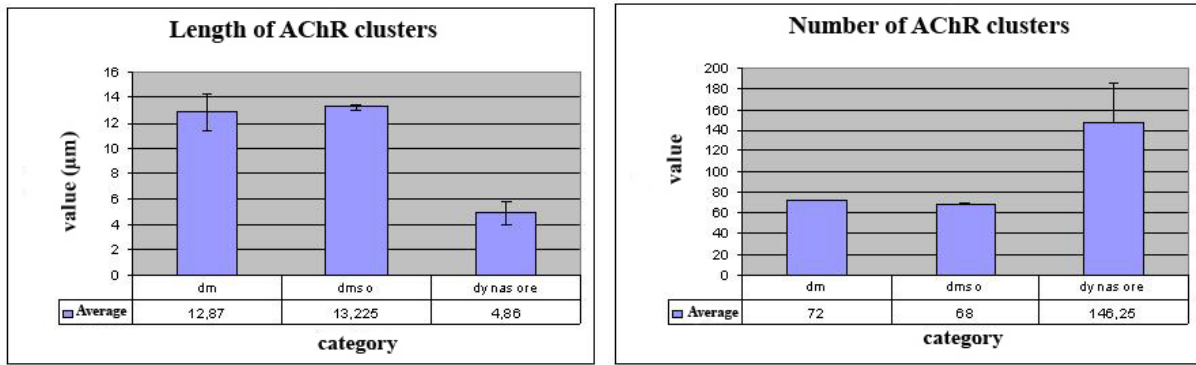
Figure 4.9: Influence of dynasore on agrin induced AChR clustering in muscle cells. Myotubes were preincubated with dynasore, DMSO, or left in DM for 30 minutes. Cells were incubated for 8 hours with agrin to induce AChR cluster formation. AChRs were stained with $\alpha$-BGT-Alexa 594. AChR clusters from 10 fields visualised with a 63X objective were counted and measured. Quantification, using the Metamorph Imaging Software (Molecular Devices) was done from 5 different samples (n=5), and results were collected from 2 independent experiments. The standard deviation (SD) is shown.

to the medium for an additional 30 minutes. Cells were lysed in RIPA buffer supplied with inhibitors, biotin-$\alpha$-BGT was added to label AChRs and AChRs were pulled down using streptavidin agarose beads. Sampels were resolved by SDS-PAGE and immunoblotted with anti-phosphotyrosine antibody ($\alpha$-PTy) and anti-AChR antibody ($\alpha$-AChR$\beta$). Agrin induced AChR phosphorylation was significantly reduced in myotubes pretreated with dynasore (figure 4.10).

A similar experiment was performed in C2C12 muscle cells, where cells were incubated with agrin for 30, 60 and 120 minutes. Figure 4.11 shows that AChR$\beta$ phosphorylation was reduced for all time intervals in cells incubated with dynasore compared with control experiments.

## 4.2 Generation of a muscle cell line expressing MuSK-SBP

In order to follow MuSK endocytosis in muscle cells, a MuSK$^{-/-}$ muscle cell line expressing SBP-tagged MuSK was generated (C3.16/MuSK-SBP). C3.16 cells are myoblasts from embryonic muscle cells of MuSK$^{-/-}$ mice. Thus they express no endogenous MuSK protein [Herbst & Burden, 2000]. A retroviral expression vector containing MuSK-SBP was constructed and MuSK$^{-/-}$ myoblasts were infected. Puromycin resistant clones were selected and tested for differentiation, MuSK expression, MuSK tyrosine phosphorylation and AChR cluster formation.
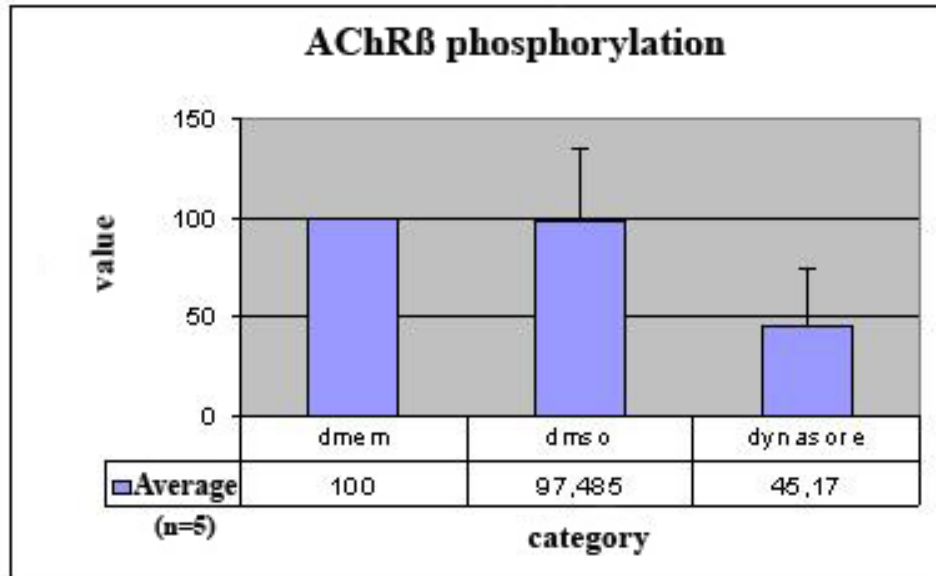
Figure 4.10: Influence of dynasore on agrin-induced AChR$\beta$ phosphorylation. C2C12 myotubes were incubated with dynasore, DMSO or DMEM for 30 minutes and than stimulated with agrin for 30 minutes. Cells were lysed and AChRs were pulled down using biotin-$\alpha$-BGT-streptavidin agarose beads. Samples were resolved by SDS-PAGE and immunoblotted with antibodies against phosphotyrosine (PTy) and AChR$\beta$. Quantification of the results was performed with BioRad Quantity One Analysis Software. The result from 5 different experiments (n=5) is shown. The phosphorylated proteins were normalised to the total amount of proteins and the results from the experiment where cells were incubated only in DMEM as 100%. The error bars represent the standard deviation (n=5).
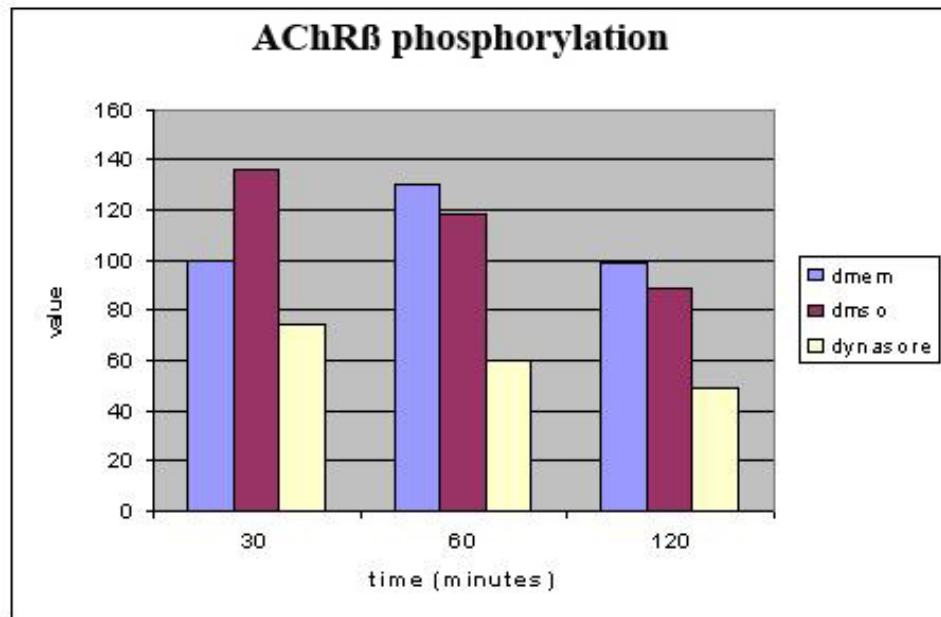
Figure 4.11: Influence of dynasore on agrin-induced AChR$\beta$ phosphorylation. C2C12 myotubes were incubated with dynasore, DMSO or DMEM for 30 minutes and than stimulated with agrin for 30, 60 and 120 minutes. Cells were lysed and AChRs were pulled down using $\alpha$-biotin-BGT-streptavidin agarose beads. Samples were resolved in SDS-PAGE and immunoblotted with antibodies against phosphotyrosine (PTy) and AChR$\beta$. Quantification of the blot was performed with BioRad Quantity One Analysis Software. The phosphorylated proteins were normalised to the total amount of proteins and the results from the experiment where cells were incubated only in DMEM for 30 min were set as 100%. In this figure are the results from one experiment.

## 4.2.1 Generation of pBabe/MuSK-SBP vector

MuSK-SBP was released from the original vector [McCann et al., 2005] using EcoRI (figure 4.12). The eluted fragment was ligated into pBabe (figure 4.13) and transformed into SURE bacteria. The bacteria were selected over night on ampicillin medium. 10 colonies were multiplied in a over night culture and the DNA plasmid was extracted using a mini-prep kit.
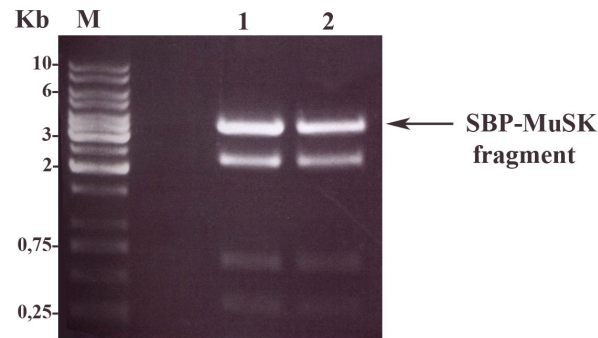


Figure 4.12: Isolation of the MuSK-SBP fragment. Enzyme digestion products (1-2) were run on agarose gel. Successful and distinctive bands of expected size ( 3400bp) can be seen, representing the desired MuSK-SBP fragment. M marker,1-2: double probes of the same enzyme digestion.

Two control digests were performed. The first one was to check the release of MuSK-SBP insert with EcoRI enzyme (figure 4.14 A). The second digest was performed to check the orientation of the insert with Bgl II and Spe I enzymes (figure 4.14 B). One sample contained the plasmid with a correct inserted MuSK-SBP fragment. The accuracy of the inserted MuSK-SBP fragment was checked by sequencing.

## 4.2.2 Selection of different cell lines

Pheonix cells, a retrovirus producer cell line, were transfected with pBabe-MuSK-SBP plasmid. Pheonix cells express the envelope proteins of the retrovirus and help to produce a functional retrovirus. The virus containing medium was used to infect MuSK$^{-/-}$ myoblasts. Infected cells were cultivated on selection medium containing puromycin. In order to select only single cell clones, cells were plated at low density. Every cell gave rise to a clone. 12 clones were picked and transfered into a multi-well dish. Each clone was tested for differentiation and MuSK expression. From the 12 cell lines only 6 developed myotubes when induced to differentiate. These lines were further used to determine MuSK-SBP expression and agrin induced MuSK phosphorylation.
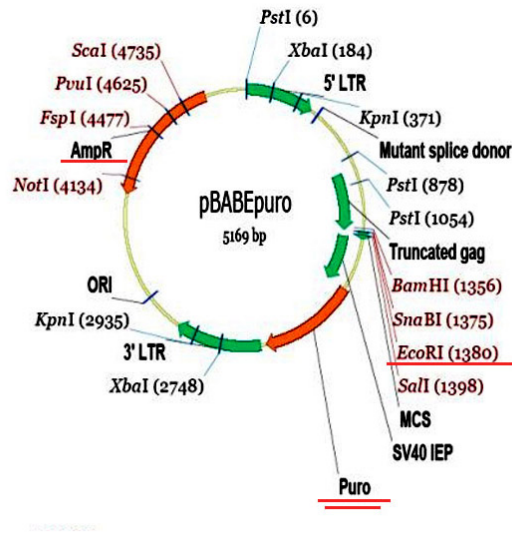
Figure 4.13: Scheme of pBabe vector. Length: 5169 bp. ORI: origin. Ampicillin and puromycin resistance.
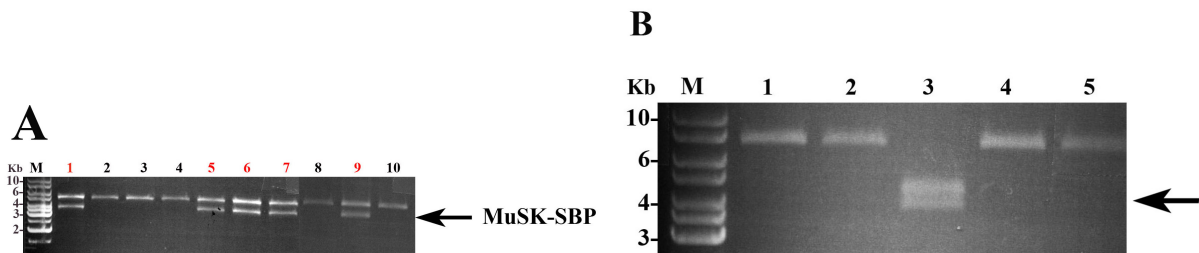


Figure 4.14: Restriction analysis of vector DNA. A, Control digest with EcoRI enzyme to check the presence of MuSK-SBP fragment. The numbers in red are the positives. The numbers in black do not contain MuSK. B, Control digest with Bgl II and Spe I enzymes to check if the MuSK-SBP fragment was inserted in the correct orientation. Digestion products (1-5) were run on an agarose gel. Only the sample number 3 was positive. M: Marker.
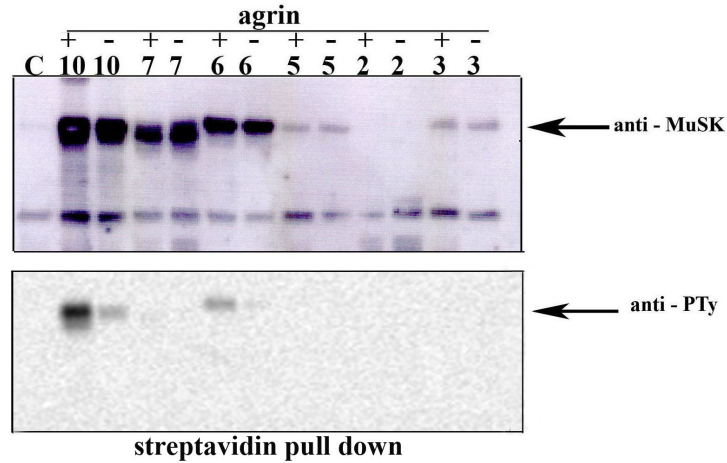
Figure 4.15: Phosphorylation and expression of MuSK-SBP in MuSK$^{-/-}$ cells. C3.16 MuSK-SBP myotubes derived from cell clones (10, 7, 6, 5, 3, 2) were stimulated with agrin (+) or kept in medium without agrin (-). MuSK-SBP was precipitated using streptavidin agarose beads, sampels were separated by SDS-PAGE and analyzed by Western immunoblot. In the first panel we can see MuSK-SBP expression, the blot was incubated with anti-MuSK antibodies and in the second panel we can see MuSK phosphorylation, the blot was incubated with antibodies against phosphotyrosine (PTy). C, control, lysates from MuSK$^{-/-}$ myotubes were used for the pull down.

### 4.2.3 MuSK expression and agrin induced MuSK phosphorylation

Parallel experiments were performed, where myotubes were stimulated for 30 min with agrin, or were kept in medium without agrin. The cells were subsequently lysed and MuSK-SBP was pulled down using streptavidin agarose beads. The isolated MuSK-SBP protein was analyzed by immunoblotting. Figure 4.15 shows, that not all cell lines expressed MuSK. Cell line number 10,7 and 6 expressed MuSK-SBP at higher levels. Most importantly MuSK-SBP is phosphorylated in response to agrin in cell line number 10 and 6. As a control for the pull down I used MuSK$^{-/-}$ myotubes that express no endogenous MuSK protein.

## 4.3 Characterisation of cell lines

### 4.3.1 Agrin induced AChR clustering in C3.16/MuSK-SBP myotubes

C3.16/MuSK-SBP myotubes were stimulated for 8 hours with agrin 4.8 or with agrin 0.0 (inactive form) to induce AChR cluster formation. Cells were fixed in 4% PFA, stained
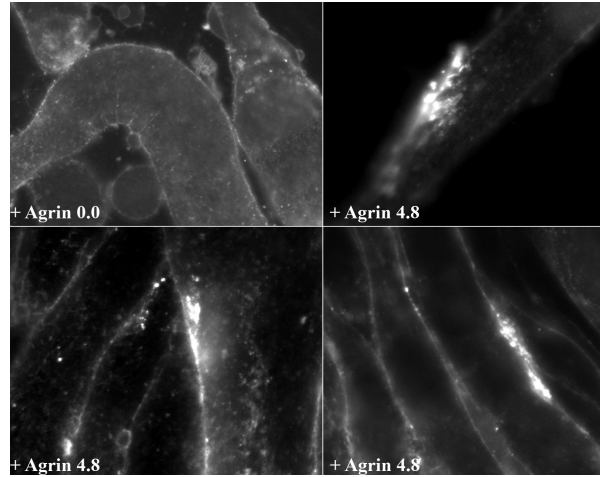
Figure 4.16: C3.16/MuSK-SBP myotubes form AChR clusters in response to agrin. AChRs were stained with $\alpha$-BGT-Alexa-594 and clusters were visualized with a fluorescence microscope. In the first panel left are shown myotubes stimulated with inactive agrin (agrin 0.0). The other 3 panels represent myotubes with agrin-induced AChR clusters.

with $\alpha$-BGT-Alexa-594 and visualized using a fluorescence microscope. Figure 4.16 shows C3.16/MuSK-SBP myotubes and agrin-induced AChR clusters. Agrin-induced AChR clusters could not be observed in myotubes treated with agrin 0.0 in contrast to myotubes treated with agrin 4.8 where AChR clusters are readily visible. I used cells derived from clone number 10, due to the high MuSK-SBP expression and due to the fact that myoblasts differentiate very well.

## 4.3.2 Time course of agrin-induced MuSK phosphorylation in C3.16/MuSK-SBP myotubes

In order to find the optimal time for agrin to induce the highest MuSK-SBP phosphorylation, I performed the following experiment: C3.16/MuSK-SBP myotubes were stimulated for different time intervals with agrin. Cells were lysed in modified RIPA buffer and MuSK-SBP was pulled down using streptavidin agarose beads. Samples were run in SDS-PAGE followed by Western blotting. Figure 4.17 shows that a 30 minutes stimulation with agrin induces the strongest MuSK-SBP phosphorylation in C3.16/MuSK-SBP myotubes. This is further supported by a quantification shown in figure 4.18.

## 4.3.3 Assembly of agrin induced AChR clusters

For a better understanding of the agrin-MuSK signaling kinetics, I performed an experiment in order to define the optimal time for agrin stimulated AChR clustering.
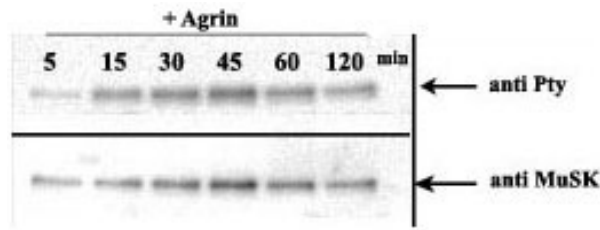
Figure 4.17: Phosphorylation of MuSK in C3.16-MuSK-SBP myotubes stimulated with agrin for different time intervals. Myotubes were stimulated for different time intervals with agrin (5-120 minutes), cells were lysed in modified RIPA buffer and MuSK-SBP was pulled down by streptavidin agarose beads. Samples were subjected to SDS PAGE and Western blot analysis, using an anti-phosphotyrosine antibody and $\alpha$-MuSK as primary antibodies.
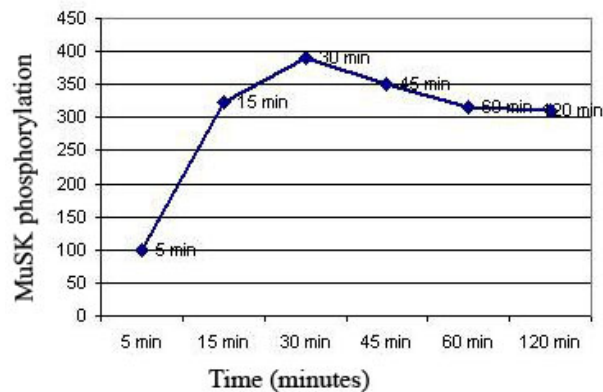


Figure 4.18: Quantification of MuSK phoshorylation after agrin stimulation for different time periods. The immunoblot from figure 4.17 was quantified using BioRad Quantity One Analysis Software.
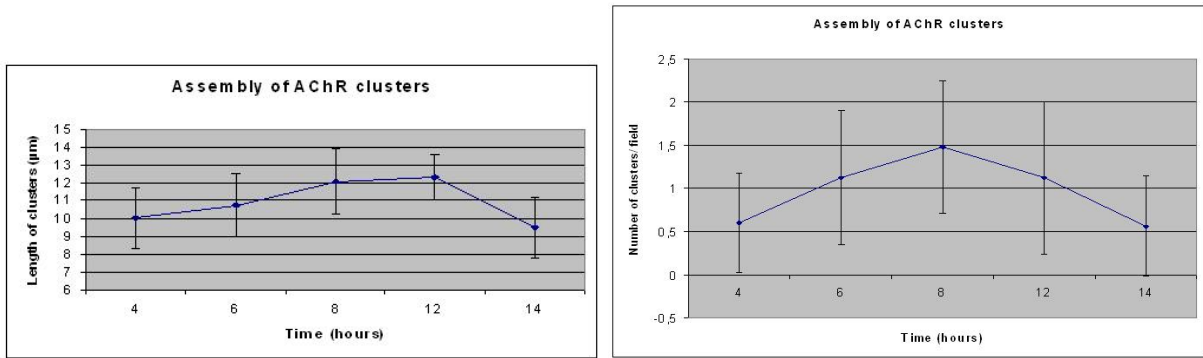
Figure 4.19: Assembly of agrin-induced AChR clusters. AChR clusters from at least 10 fields visualised with a 63X obiective were counted and measured, using the Metamorph Imaging Software (Molecular Devices) and the quantification was finalised with Microsoft Excel. The standard deviation (SD) is shown.

C3.16/MuSK-SBP myotubes were stimulated for different time intervals with agrin. Cells were fixed and AChR were stained with $\alpha$-BGT-Alexa-594. Samples were analysed with a fluorescence microscope. The number and length of clusters were counted in more than 10 fields per plate representing one time point. The highest number of agrin induced AChR clusters is obtained after 8 hours of agrin-stimulation and the longest agrin-induced AChR clusters are obtained after a stimulation with agrin from 8 to 12 hours (figure 4.19).

## 4.4 Colocalisation of MuSK and AChR in agrin induced clusters

C3.16/MuSK-SBP myotubes were stimulated with agrin for 8 hours to induce AChR cluster formation. Afterwards cells were fixed and MuSK-SBP was stained with SA-Alexa 488 and AChRs with $\alpha$-BGT-Alexa-594. Sampels were examined with a fluorescence microscope. The colocalisation between MuSK-SBP and AChRs is schown in the figure 4.20.
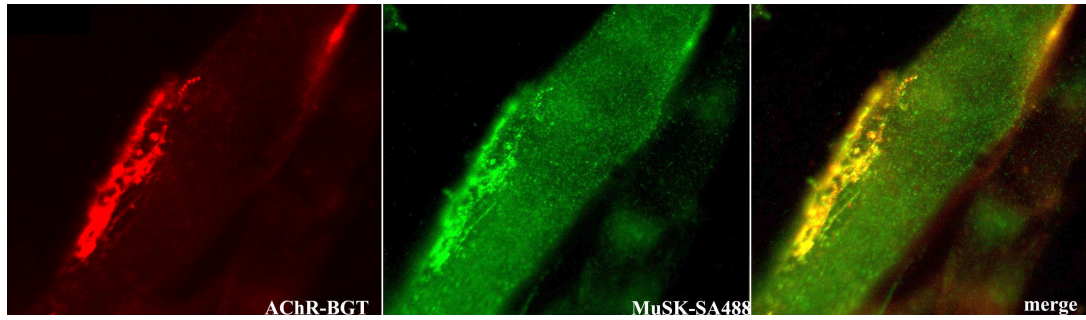
Figure 4.20: Colocalisation of MuSK-SBP and AChR clusters in agrin stimulated myotubes. AChR are stained with $\alpha$-BGT-Alexa-594, MuSK is stained with SA-Alexa 488, last panel: merge between the first 2 panels. Yellow color represents AChR and MuSK colocalisation

## 4.5 Internalization of MuSK in C3.16/MuSK-SBP myotubes

### 4.5.1 MuSK, AChRs and Cholera-toxin-stained lipid rafts at the NMS

It was previously shown that agrin stimulates a dynamic translocation of the AChR into lipid rafts-cholesterol and sphingolipid-rich microdomains in the plasma membrane [Pato et al., 2008]. This follows MuSK partition into lipid rafts and requires its activation [Zhu et al., 2006]. Fluorophores conjugated to cholera-toxin B-subunit (CT-FITC), which binds to the lipid raft constituent ganglioside GM1 can be used to visualise lipid rafts. Using CT-FITC I tried to visualize MuSK-SBP and AChRs distribution in the lipid raft platform in agrin stimulated muscle cells. For this purpose, C3.16 MuSK-SBP myotubes were stimulated for 8 hours with agrin to induce AChR clustering. Cells were stained at 10°C with $\alpha$-BGT-Alexa-594, CT-FITC and SA-Cy5. Cells were washed for 5 minutes in PBS to reduce background staining, and then fixed in 4 % PFA and mounted with Vectashield Mounting Medium. Sampels were visualized with a fluorescence microscope. Figure 4.21 shows a colocalisation between AChRs marked by $\alpha$-BGT-594 and MuSK-SBP marked by SA-Cy5 within lipid rafts marked by CT-FITC.

### 4.5.2 Colocalisation of MuSK-SBP with EEA1 early endosomes at the NMS

MuSK-SBP receptor can be specifically stained with SA (StreptAvidin) conjugated with different fluorophores and its internalization followed in C3.16/MuSK-SBP myotubes. Different endosome markers are commercially available and this offers another important
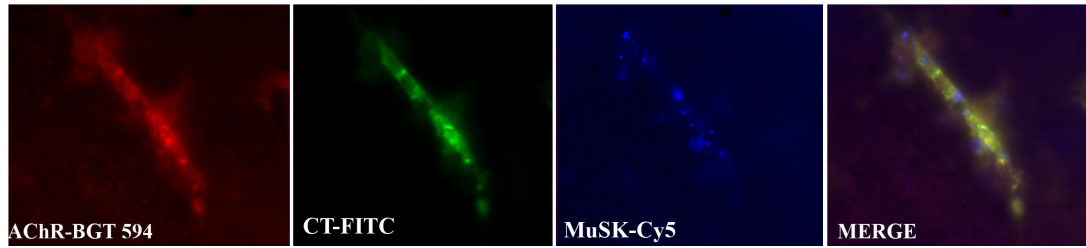
Figure 4.21: Colocalisation of lipid rafts, AChR clusters and MuSK-SBP in myotubes. AChRs are stained with $\alpha$-BGT-Alexa-594 (red), lipid rafts are stained with CT-FITC and MuSK-SBP stained with SA-Cy5(blue). Yellow color represents AChR-$\alpha$-BGT-Alexa-594 and lipid rafts-CT-FITC colocalisation.

tool in characterising MuSK endocytosis in muscle cells. We can specifically stain different endocytic compartments (Rab5, EEA1, etc.) and visualise the possible colocalisations between internalised MuSK-SBP and the specifically labeled endosomes. C3.16/MuSK-SBP myotubes were stained at 37°C for one hour with SA-488. Cells were stimulated with agrin for 10 minutes to accelerate MuSK internalization. Cells were fixed in 4 % PFA and EEA1 early endosomes were stained as described in Materials and methods. Sampels were mounted in Vectashield and visualised with a fluorescence microscope. Some possible colocalisation between MuSK-SBP and EEA1 early endosomes can be observed in figure 4.22.
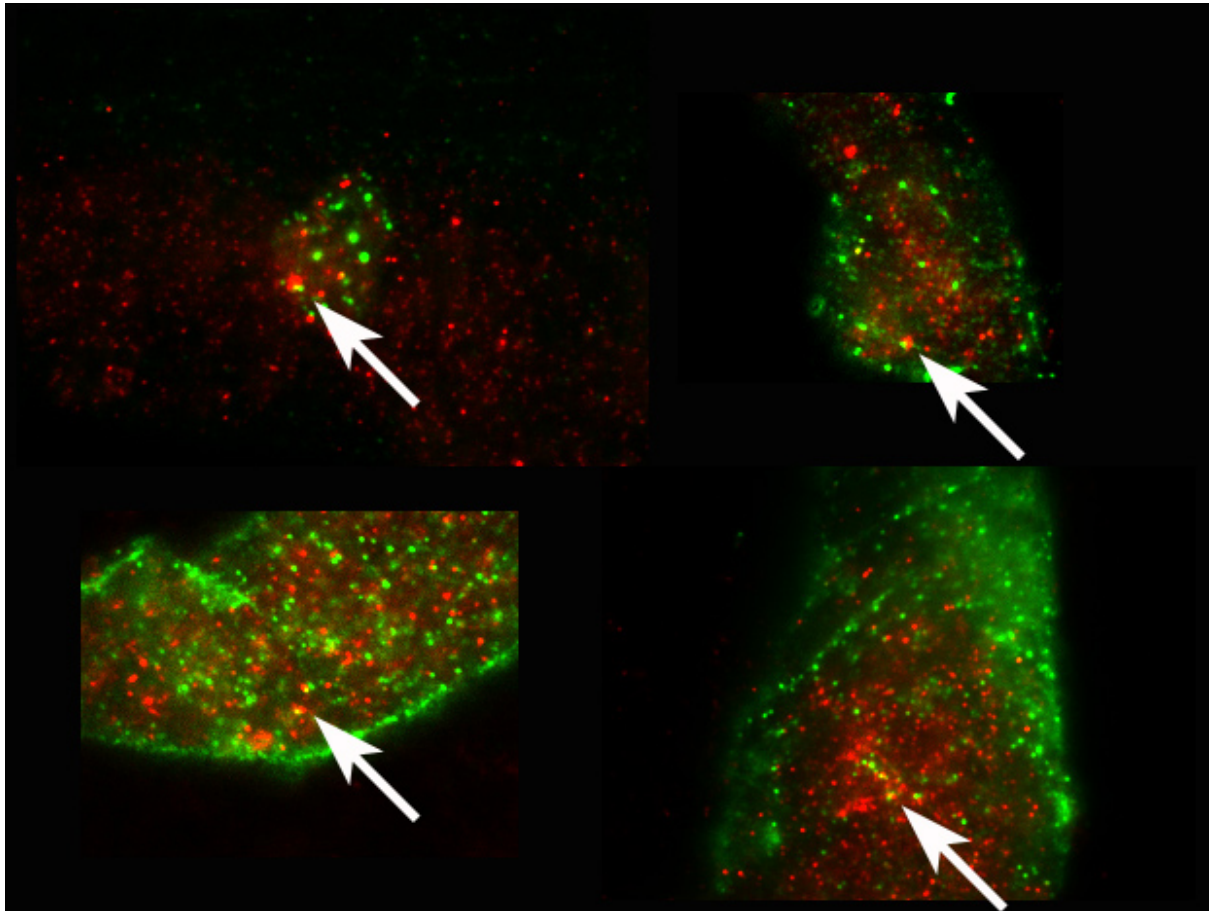
Figure 4.22: Colocalisation of MuSK-SBP with EEA1 early endosomes. All four images represent regions in C3.16/MuSK-SBP myotubes where MuSK-SBP is stained with SA-488 (green) and EEA1 early endosomes with Cy3 (red). Possible colocalisations (yellow dots) between internalised MuSK and EEA1 endosomes are indicated by arrows.

# Chapter 5

# Discussion

## 5.1 Influence of dynamin on MuSK endocytosis and signaling

### 5.1.1 Influence of dynamin 1 on MuSK endocytosis

Dynamin 1 is a neuron-specific guanosine triphosphatase thought to be critically required for the fission reaction of synaptic vesicle endocytosis. However, dynamin 1 was found to influence endocytosis processes not only in neuronal cells. For example, in polarized epithelial MDCK cells, dynamin 1 and dynamin 2 share endocytic functions depending on their localisation at the plasma membrane [Altschuler et al., 1998]. Clathrin-coated vesicle process is mediated by dynamin-1, whereas the slower form of endocytosis is mediated by dynamin-2. In my work I could show that MuSK endocytosis in HeLa cells is not dynamin 1 dependent. My findings are consistent with the fact that Eps15 mutants were unable to inhibit MuSK endocytosis when expressed in HeLa cells but inhibited the internalisation of transferrin (Susan Luiskandl, unbublished data). Eps15 (Epidermal growth factor receptor pathway substrate 15) is a protein present at clathrin-coated pits and is involved in receptor-mediated endocytosis [Benmerah et al., 1998]. It was also shown that MuSK does not colocalise with transferrin in HeLa cells. All these data suggest that MuSK endocytosis in HeLa cells is not dependent on dynamin 1 function and occurs independent of clathrin-coated pits.

### 5.1.2 Influence of dynamin 2 on MuSK endocytosis

Dynamin 2 is thought to control receptor-mediated endocytosis in virtually all somatic cells, as it is ubiquitously distributed and this form of endocytosis is universal. The first isoform of dynamin 2, dynamin 2a, is implicated in caveolar uptake from the plasma mem-

brane since a dominant negative mutant interferes with this type of internalization. The second isoform, dynamin 2b appears instead to be involved in the known "'kiss-and-run"' interactions between caveosomes and early endosomes [Mukherjee et al., 2006]. "'Kiss-and-run"' is a mode of membrane fusion and retrieval without the full collapse of the vesicle into the plasma membrane. Expression of dynamin 2a K44A, greatly inhibited MuSK endocytosis in HeLa cells, suggesting a role of dynamin 2 in MuSK endocytosis. Though, this finding does not elucidate whether MuSK endocytosis is caveolar, small GTPases (Rho A), actin, Arf6 or flotillin-1 dependent since dynamin 2a is involved in all of this types of endocytic mechanisms. To confirm the role of dyn 2, I used dynasore, which is a dynamin inhibitor. It inhibits both dynamins involved in endocytosis. My findings showed that dynasore also blocks MuSK endocytosis in HeLa cells. Even if dynasore does not resolve the question which dynamin isoform is involved in an endocytic mechanism, because it blocks all dynamin isoforms, it sustains the finding that dynamin 2 is important for MuSK endocytosis in HeLa cells.

Expressing a dominant negative dynamin mutant, in this case dynamin-2a K44A could also have non-speciffic effects, such as an increase in endosomal pH [Huber et al., 2001], whereas dynasore has been shown to cause no or little unspecific side-effects. It was previously shown that agrin induces rapid internalization of MuSK in muscle cells [Zhu et al., 2008]. Agrin induced activation of MuSK can be mimiced in HeLa cells using a constitutively active MuSK mutant. My experiments showed that endocytosis of active MuSK in HeLa cells was also blocked when cotransfected with dynamin-2a K44A indicating that active and inactive MuSK are internalised by the same endocytic machinery. It has been proposed that dynamin plays an important role in tyrosine kinase receptor-mediated signal transduction. In support of this hypothesis, dynamin has recently been shown to co-precipitate with a number of receptor tyrosine kinase, including the epidermal growth factor receptor [Seedorf et al., 1994] and the insulin receptor/insulin receptor substrate I complex [Ando et al., 1994] via joint interactions with Grb2. Dynamin is complexed with Grb2 in the absence or presence of growth factors, but becomes associated with the respective tyrosine-phosphorylated receptor only upon growth factor stimulation [Seedorf et al., 1994]. In addition, Scaife et al. [Scaife et al., 1994] report that the association of dynamin with phospholipase C and the platelet-derived growth factor receptor is further increased with growth factor stimulation [Urrutia et al., 1997].

### 5.1.3 The role of dynamin during AChR clustering

Other important findings of my diploma thesis showed that dynasore reduces agrin induced clustering in muscle cells as well as agrin induced AChR beta-subunit phosphorylation. This results are in concordance with the findings of [Zhu et al., 2008]. The

researchers showed that inhibition of MuSK endocytosis, by expressing dynamin-K44A attenuates agrin-induced AChR clustering in muscle cells. They also showed that MuSK undergoes rapid endocytosis after agrin stimulation, very much like other receptor tyrosine kinases such as EGFR (epidermal growth factor receptor) and ErbB4, which are known to internalize after ligand stimulation [Vieira et al., 1996, Yang et al., 2005]. All this findings suggest an important influence of MuSK endocytosis on agrin-induced MuSK signaling.

The partition of MuSK into lipid rafts increases after agrin stimulation, and this translocation depends on its tyrosine kinase activity [Zhu et al., 2006]. The dynamic behavior of MuSK into lipid rafts is most analogous to other RTKs, including TrkB [Suzuki et al., 2004], c-Ret [Paratcha & Ibáñez, 2002], and ErbB4 [Ma et al., 2003]. Once stimulated by the respective ligand, these transmembrane kinases translocate into lipid rafts, and such translocation is necessary for signaling. Remarkably, MuSK translocation to rafts is followed by the recruitment of the AChR, suggesting a sequential signal transduction within lipid rafts. Importantly, lipid raft disruption, either by removing cholesterol from the membrane or by reducing the glycosphingolipid level, inhibits MuSK signaling, including MuSK phosphorylation, AChR beta-subunit phosphorylation, and activation of the Rac1 GTPases [Zhu et al., 2006]. Therefor it appears possible that a ligand-dependent turnover of MuSK via lipid rafts takes place and this turnover could be important for the recruitment and stability of AChR clusters.

Upon agrin engagement, actin and actin-nucleation factors such as Arp2/3 and N-WASP were transiently recovered within raft fractions suggesting that the activation by agrin can trigger actin polymerization [Pato et al., 2008]. Therefor, the present data suggest that AChR clustering at the neuromuscular junction relies upon a mechanism of raft coalescence driven by agrin-elicited actin polymerization. Dynamin may regulate actin filaments coordinately with its activities that remodel membranes [Schafer, 2004]. So, dynasore might also lead to a reduction of the agrin-MuSK signaling in muscle cells, due to the blockage of dynamin that perturbs actin polymerization and destabilises the entire mechanism of AChR clustering.

## 5.2 Internalization of MuSK in MuSK$^{-/-}$/MuSK-SBP myotubes

The generation of a muscle cell line expressing a SBP-tagged MuSK, enables the visualisation of MuSK receptor and its internalization at the NMS. AChR is present in nonraft microdomains in naive muscle cells and the cluster formation is detectable by 4 h and is maximal after 8 h of agrin stimulation in lipid rafts. I could show that, after 8 hours of agrin stimulation, MuSK colocalises with AChR clusters at the level of lipid raft platform marked with CT. This finding is consistent with other discoveries [Zhu et al., 2006] showing that agrin-induced AChR clusters colocalise with lipid rafts in muscle cells. We are interested in the visualisation of MuSK distribution upon agrin-stimulation. In my study I was able to show a partial colocalisations of MuSK with EEA1 (early endosome antigen 1) positive early endosomes after a 10min stimulation with agrin. EEA1 early endosomes are found in clathrin-dependent internalization as well as in lipid raft internalization pathways.

Endocytosis of cell surface receptors is an important regulatory event in signal transduction. For example, TGF-beta receptors internalize into both caveolin- and EEA1-positive vesicles and reside in both lipid raft and non-raft membrane domains. Clathrin-dependent internalization into the EEA1-positive endosome, where the Smad2 anchor SARA is enriched, promotes TGF-beta signaling. In contrast, the lipid raft-caveolar internalization pathway contains the Smad7-Smurf2 bound receptor and is required for rapid receptor turnover. Thus, segregation of TGF-beta receptors into distinct endocytic compartments regulates either Smad activation or receptor turnover [Di Guglielmo et al., 2003].
Another example where endocytosis plays an important role in signaling is represented by ErbB tyrosine kinases which become rapidly internalized in response to its ligand neuregulin. The internalization requires the kinase activity of ErbB and involves a clathrin-dependent endocytic pathway. Moreover, neuregulin-induced Erk activation and AChR expression were attenuated when ErbB endocytosis was blocked. These results indicate that ErbB proteins undergo endocytosis in response to neuregulin, and this process is required for neuregulin signaling and induced AChR expression [Yang et al., 2005].
Taken together, accumulating evidence suggests a tight cross-talk between signaling and endocytosis. Thus it will be of great importance to study MuSK endocytosis in more detail to elucidate its influence on MuSK signaling.

## 5.3  Outlook

In future experiments, MuSK endocytosis will be further characterized. There are various methods to detect if a receptor is internalised via a clathrin-dependent or -independent endocytosis. For example, we can block clathrin-independent endocytic pathways using $\beta$-methylcyclodextrin or nystatin that leads to cholesterol depletion. As control for this experiment we can perform a sucrose density gradient centrifugation or staining with CT that should not bind anymore if lipid rafts are depleted. We could express dominant-negative mutants of caveolin, flotillin, Rho A and other proteins involved in different endocytic pathways. Alternatively, these proteins can be down-regulated using siRNA. These experiments should be performed in HeLa cells as well as in other type of cells that are richer in lipid rafts, for example in fibroblasts.

On the other hand, the clathrin dependent endocytosis can be disturbed by interfering with several accessory proteins that are implicated in the formation of clathrin-coated vesicles, as indicated by their ability to interact with other endocytic components like clathrin and AP-2 (adaptor protein 2) [Mousavi et al., 2004]. Expression of fragments of these proteins that contain functional domains, inhibit clathrin-dependent endocytosis. A mutant AP-2 lacking a functional phosphoinositide binding site acts as a dominant-negative inhibitor of coated pit formation [Owen et al., 2004]. Exposing live cells to hypertonic sucrose can also inhibit clathrin-mediated endocytosis [Heuser, 1989].

Other future plans will concentrate on the muscle cell line expressing the SBP tagged MuSK. MuSK internalization will be followed and the possible colocalisation with different endocytic compartments will be studied. We can specifically stain early and late endosomes, as well as lysosomes and Golgi apparatus. We can also use tagged proteins, like flotillin-GFP or caveolin-GFP and see if there are colocalisations with MuSK. Another future plan is to see the influence of ubiquitin on the endocytosis pathways [Sigismund et al., 2005].

A very important future plan is to study MuSK distribution at the NMS compared with AChR clusters in the presence or absence of agrin. This could lead to a better understanding of MuSK localisation and function during NMS assembly and disassembly and could answer the question whether MuSK is internalised before reaching the lipid rafts, or the translocation occurs due to a horizontal movement within the plasma membrane.

# Chapter 6

# Materials and methods

## 6.1  Chemical Reagents

| | |
|---|---|
| 10xPBS | Gibco |
| 40% Acrylamide | Roth |
| Acetic acid | Roth |
| Agar-Agar | Roth |
| Alexa 488 Conjugated Streptavidin | Invitrogen |
| Alexa 594 Conjugated Streptavidin | Invitrogen |
| Ampicillin | Roth |
| APS | Roth |
| BSA | Roth |
| Bromphenolblue | Roth |
| Calcium chloride | Roth |
| Cholera Toxin B Subunit from Vibrio cholerae FITC Conjugate | Sigma-Aldrich |
| Cy3 Conjugated Streptavidin | Jackson ImmunoResearch |
| Cy3 Conjugated AffiniPure Donkey Anti-Mouse IgG | Jackson ImmunoResearch |
| Cy5 Conjugated Streptavidin | Jackson ImmunoResearch |
| Dynasore monohydrate | Sigma-Aldrich |
| DMEM | Sigma |
| DMSO | Roth |
| EDTA | Promega |
| Ethanol | Roth |

| | |
|---|---|
| Ethidium bromide | Roth |
| FBS | Sigma |
| Gelatin | Sigma |
| Glycerol | Roth |
| Glycine | Promega |
| HCl | Roth |
| Iodoacetamide | Sigma |
| Isopropanol | Roth |
| Kanamycin | Roth |
| LB-broth | Roth |
| Lumi Light | Roche |
| Methanol | Roth |
| MgCl2 | Roth |
| MgSO4 | Roth |
| Midi prep kit | Invitrogen |
| Mini prep kit | Fermentas |
| Modifying enzymes | Fermentas |
| NaOH | Roth |
| NP-40 | Sigma |
| OptiMem | Gibco |
| Paraformaldehyde | FLUKA |
| Penicillin/Streptomycin | Sigma |
| Phenol/Chloroform | Roth |
| PEG | Roth |
| Potassium chloride | Roth |
| Prestained protein ladder | Fermentas |
| Protein A-agarose | Roche |
| Purified Mouse Anti-EEA1 | BD Transduction Laboratories |
| Restriction enzymes | Fermentas |
| Rhodamine Conjugated Human Transferrin | Rockland |
| Silicone glass wool | Bertoni |
| Sodium acetate | Roth |
| Sodium chloride | Roth |
| Sodium dodecyl sulfate | SERVA |
| Sodiumdihydrogen phosphate | Roth |
| Sodiumfluoride (NaF) | Fluka Chemika |
| Sodiumhydrogen phosphate | Roth |

| | |
|---|---|
| Streptavidin Agarose | Novagen |
| streptavidin and Fluorescent Conjugates of Streptavidin | Invitrogen |
| Texas-red-$\alpha$-bungarotoxin | Molecular Probes |
| Tris | Roth |
| Triton X-100 | Sigma |
| Trypsin-EDTA | Gibco |
| Tween 20 | Promega |
| Vectashield | VECTOR |
| $\alpha$-MuSK antibody | R. Herbst ([Herbst & Burden, 2000]) |
| $\alpha$-phosphotyrosine antibody | (Cell Signaling p100; Santa Cruz p99) |
| $\alpha$-bungarotoxin, Alexa Fluor 594 conjugate | Molecular Probes |
| $\beta$-Mercaptoethanol | Roth |

## 6.2   Plasmids

| Plasmid name | Description/Cloning | Reference |
|---|---|---|
| pRK5-dyn 1 K44A | The cDNA encoding dynamin 1 K44A was isolated from pTM1 by Bam H1 and Hind III digestion and subcloned into pRK5 vector. | Hanna Damke |
| pRK5-dyn 1 WT | The cDNA encoding dynamin 1 WT was isolated from pTM1 by Bam H1 and Hind III digestion and subcloned into pRK5 vector. | Hanna Damke |
| pEGFP-N1-Dyn2(aa)-K44A | pEGFP/N is a mammalian expression vector that encodes a red-shifted variant of wild-type GFP. A gene of interest inserted into the MCS of this vector will be expressed as a fusion to the N-terminus of GFP. | Ari Helenius |
| pEGFP-N1-Dyn2(aa)-WT | pEGFP/N is a mammalian expression vector that encodes a red-shifted variant of wild-type GFP. A gene of interest inserted into the MCS of this vector will be expressed as a fusion to the N-terminus of GFP. | Ari Helenius |
| pBabe-MuSK-SBP | The cDNA encoding MuSK-SBP was released from the original vector [McCann et al., 2005] using EcoRI and subcloned into pBabe vector | [McCann et al., 2005] |
| pBabe-MuSK-SBP-KA | The cDNA encoding MuSK-SBP KA was subcloned into pBabe vector | Susan Luiskandl |

## 6.3 Plasmid preparation

### 6.3.1 Small scale plasmid preparation

1.5-3 ml of an overnight culture (in LB medium containing $50\mu$g/ml Ampicillin or $30\mu$g/ml Kanamycin) were centrifuged at maximum speed in an Eppendorf 5415 D centrifuge and plasmids were isolated using the Fermentas GeneJetTM Plasmid Miniprep kit. All steps were carried out as recommended by the manufacturer.

### 6.3.2 Large scale plasmid preparation

150ml of an overnight culture (in LB medium containing $50\mu$g/ml Ampicillin or $30\mu$g/ml Kanamycin) were centrifuged at 3500rpm in an Eppendorf 5804 centrifuge using the A-4-44 swinging-bucket rotor. Plasmids were isolated using the Invitrogen Pure LinkTM HiPure Plasmid Filter Purification Kits Midiprep kit. All steps were carried out as recommended by Invitrogen. The DNA concentration was determined by measuring an aqueous dilution at 260nm.

## 6.4 Manipulation of DNA with enzymes

### 6.4.1 Restriction enzyme digestion

Enzymes were supplied by Fermentas or New England Biolabs and used as suggested by the manufacturer. Digestions were mostly carried out in a $20\mu$l volume using 0.5-1$\mu$l restriction enzyme solution and approximately 0.5 to 1$\mu$g of DNA.

### 6.4.2 Ligation of DNA

Ligation reactions were always carried out in a $20\mu$l volume with a molar ratio of vector to insert of approximately 1:3, except for very small inserts, which were used in higher excess. Prior to ligation, vector and insert were digested with restriction enzymes that produced the same or compatible cohesive ends. The ligation was performed by combining vector and insert DNA in an Eppendorf tube and adding 1$\mu$l T4 DNA ligase (5u/$\mu$l), 2$\mu$l 10x T4 buffer and dH2O up to $20\mu$l. After an incubation of 2h at RT, the whole ligation mix was transformed into competent bacteria.

### 6.4.3   Dephosphorylation of DNA

For dephosphorylation of linearized plasmids 1 $\mu$l of SAP (shrimp alkaline phosphatase, 1u/$\mu$l) was added right after digestion, followed by a 1h incubation period at 37°C.

## 6.5   Isolation of DNA restriction fragments

Digested DNA was run on a 0.7-2% agarose gel/1xTAE containing 2$\mu$l EtBr per 50ml of gel. The bands were visualized by UV. DNA containing agarose blocks were cut out and centrifuged against a plug of siliconized glass wool. Then a phenol/chloroform extraction was carried out by adding 1 volume phenol/chloroform, centrifugation for 5min at maximum speed in a table-top centrifuge and removal of the upper phase. Finally, the DNA was precipitated with 3 volumes of ethanol/0.3M sodium acetate and washed with 70% ethanol. The pellet was dissolved in TE and stored at -20°C or used immediately for ligation. Concentrations of isolated DNA fragments were estimated by loading 1$\mu$l aliquots onto an agarose gel and comparing the resulting bands to the marker, that was loaded at known concentration.

## 6.6   Transformation of competent bacteria

In an Eppendorf reaction tube 20 $\mu$l ligation mix, 20 $\mu$l 5xKCM buffer, 60 $\mu$l dH2O and 100 $\mu$l competent bacteria were mixed. Then the tube was placed on ice for 30min, afterwards on 42°C for a 2min heat shock and then put back on ice again. After the addition of 900 l LB medium without antibiotics the tube was incubated at 37°C in a water bath for 30min. Then the cells were pelleted and 1ml of the supernatant was discarded. The pellet was resuspended and plated on selection media.

| 5x KCM buffer: | 0.5M KCl |
| --- | --- |
| | 0.15M CaCl2 |
| | 0.25M MgCl2 |

## 6.7   Protein gel electrophoresis and western blot analysis

Different percentage polyacrylamid gels were prepared, according to the size of proteins to be analyzed. Samples were loaded into the gel slots and gels were run at 140-180V in

1xRunning Buffer. After separation of the proteins, the gels were removed from the electrophoresis apparatus and immediately put into transfer buffer. For Western blot analysis the gel was placed on top of a PVDF-membrane (which was incubated in methanol and washed with transfer buffer right before) between two transfer buffer-drained papers in a blotting apparatus and a current of 50mA was applied per gel. The proteins were allowed to transfer to the membrane for 1h. Afterwards, the membrane was immediately put into TBS-Tween for washing. For further analysis the membrane has to be blocked. This was achieved by incubating the membrane for 2h on a shaker at room temperature in a 5% BSA/TBS-Tween solution. The primary antibody in 5% BSA + 0.1% NaN3 in TBS-Tween, was added to the membrane. After 1h at RT or overnight incubation at 4°Cthe membrane was washed 3 times with TBS-Tween and then the secondary horse reddish peroxidase conjugated antibody, diluted in 5% instant milk powder in TBS-Tween, was added. After 1h, the membrane was washed 3 times and incubated with Roche Lumi-Light. The bands were visualized by subjecting the membranes to BIO-RAD Fluor-STM MultiImager. Bands were analyzed using BIO-RAD Quantity One - 4.1.1 Software. To remove the antibody binding, blots can be stripped in 10% acetic acid for 2h on a shaker and afterwards washed 3 times with water. Then the blots could be reused for another antibody reaction.

### 6.7.1  Solutions and gels

5xRunning Buffer:   15.05g Tris base
                    72 g glicine
                    dissolved in almost 1l dH2o
                    5g SDS were added and the volume adjusted to 1l

Transfer Buffer:    25mM Tris pH 8
                    192mM glycine
                    20% methanol

| PAA-Gels | running gel | | | | | | | | |
|---|---|---|---|---|---|---|---|---|---|
| | 7.5% | | | 10% | | | 12.5% | | |
| total volume [ml] | 5 | 10 | 20 | 5 | 10 | 20 | 5 | 10 | 20 |
| 40% AA mix [ml] | 0.94 | 1.88 | 3.76 | 1.25 | 2.5 | 5 | 1.55 | 3.1 | 6.2 |
| 1.5M Tris/0.5M HCl [ml] | 1.25 | 2.5 | 5 | 1.25 | 2.5 | 5 | 1.25 | 2.5 | 5 |
| $dH_2O$ [ml] | 2.7 | 5.4 | 10.8 | 2.4 | 4.8 | 9.6 | 2.1 | 4.2 | 8.4 |
| 10% SDS [μl] | 50 | 100 | 200 | 50 | 100 | 200 | 50 | 100 | 200 |
| APS [μl] | 50 | 50 | 100 | 50 | 50 | 100 | 50 | 50 | 100 |
| TEMED [μl] | 5 | 10 | 20 | 5 | 10 | 20 | 5 | 10 | 20 |

| PAA-Gels | stacking gel | |
|---|---|---|
| | 5% | |
| total volume [ml] | 5 | 10 |
| 40% AA mix [ml] | 0.625 | 1.25 |
| 0.02M Tris/0.48M Tris.Cl [ml] | 1.25 | 2.5 |
| $dH_2O$ [ml] | 3.025 | 6.05 |
| 10% SDS [μl] | 50 | 100 |
| APS [μl] | 50 | 100 |
| TEMED [μl] | 5 | 10 |

# 6.8 Cell culture

## 6.8.1 HeLa cell line

HeLa cells were grown in DMEM supplemented with 10% FBS and 1% penicillin/streptomycin (=general medium, GM). The incubator was adjusted to 37°C and 6% CO2. Cells were split every second day when they were about 80-90% confluent.

## 6.8.2 C2C12 cells

C2C12 cells were grown in DMEM supplemented with 15% FBS, 0.25% chicken embryonic exctract and 1% penicillin/streptomycin (=general medium, GM). The incubator was set to 37°C and 6% CO2. Cells were split every two days when they were about 80-90% confluent. For differentiation of C2C12 myoblasts into myotubes cells were plated ( $1.3*10^5$ cells / 3.5cm dish) on gelatine coated dishes and switched to DMEM supplemented with 2% HS and 1% penicillin/streptomycin (=differentiation medium, DM) at 90% confluency. DM was changed every 24 hrs. for 3 days until myotube formation was accomplished.

### 6.8.3   C3.16 mutant cell line

The C3.16 ($MuSK^{-/-}$ ) cell growth induced by large T oncogene expression requires expansion of this cell line at 33°C and 6% CO2. Cells were grown on gelatine coated dishes in DMEM supplemented with 10% FBS, 10% HS, 0.25% chicken embryonic exctract, $200\mu l$ IFN-$\gamma$ / 100ml GM and 1% penicillin/streptomycin (=general medium, GM). For differentiation of C3.16 myoblasts into myotubes cells were plated ( $1*10^6$ cells / 10cm dish) on matrix gel coated dishes. Cells were switched to DMEM supplemented with 10% FBS, 10% HS and 1% penicillin/streptomycin (=differentiation medium, DM) at  100% confluency and moved to 37°C and 6% CO2. DM was changed every 24 hrs. for  3 days until myotube formation was accomplished. In the case of C3.16/MuSK-SBP cell lines, GM was supplemented with puromycin $10\mu l$ / 100ml GM.

### 6.8.4   Freeze cells

A 10cm plate of happily growing cells that were about 60-70% confluent was trypsinized. The cells were washed off the plate with 5ml GM, then centrifuged for 5min at 1500rpm. The cell pellet was well resuspended in 1ml freeze medium (GM + 10% DMSO). Cells were frozen at -80°C and subsequently put into a liquid nitrogen for longtime storage.

## 6.9   Transfection of HeLa cells by Ca2+ DNA precipitation

HeLa cells were cultured on glass coverslips (20mm diameter) and the coverslips were placed in a 6-well dish. 2x BBS and the 0.25M CaCl2 solutions were thawed quickly and placed at room temperature. For every 3.5 cm plate from the 6-well dish, 4-5 $\mu$g DNA were used and pipetted into a round bottom polystyrene tube. Then, 175 $\mu$l 0.25M CaCl2 were added and the solution was vortexed. Afterwards, 175 $\mu$l 2xBBS were added and the tube was vortexed again, followed by incubation at room temperature for 13-15min. After this incubation step, the DNA mix was added drop-wise on top of the cells. 12-15h after transfection, the growth medium was changed to remove the precipitate and let the cells recover In case of cotransfection, 3 $\mu$g DNA of MuSK-SBP and 2 $\mu$g DNA of dynamin plasmid were used for every 3.5 cm dish.

2XBBS:  80ml sterile ddH2O

        5.6ml 5M NaCl

        5.0ml 1M BES

        $150\mu$l 1M Na2HPO4

        pH adjusted to 6.95

        volume raised to 100ml

## 6.10    Lysates of HeLa / C2C12/ C3.16 cells

Cells ready for processing were put on ice and the growth medium was aspirated. The cells were washed twice with ice-cold PBS. Afterwards, RIPA lysis buffer containing protease inhibitors was added (1ml per 10cm plate, $500\mu$l per 6 cm plate). For lysis to occur, plates were left on a shaker at 4°C for 30min. Then the cells were scraped off each plate and transferred into an Eppendorf tube. Lysates were centrifuged at 4°C for 10min at maximum speed in an Eppendorf 5415 D centrifuge. The supernatants were transferred into new centrifuge tubes. Samples were either used immediately for further analysis or frozen in liquid nitrogen and stored at -80°C. Protease inhibitors Leupeptin, Pepstatin, Orthovanadate phosphatase, Aprotinin and PMSF were added to the lysis buffer right before usage.

RIPA Buffer:  50 mM Tris-HCl, pH 7,5

        150 mM NaCl

        1% NP-40

        0,5% DOC

        50 mM NaF

        dissolved in almost 200ml dH2o

        volume adjusted to 200ml

## 6.11    Immunoprecipitation

Cell lysate aliquots of 500 $\mu$l were incubated with the respective antibody at 4°C on a rotating device. After 15 hrs. incubation 20 $\mu$l protein A agarose beads was added and incubated for 1 hr. on a rotating device at 4°C. Lysates were centrifuged for 1 min at maximum speed in an Eppendorf 5415 D centrifuge. The protein A agarose beads were washed 3 times using 1 ml of ice cold Ripa lysis buffer containing protease inhibitors. Bound proteins were eluted with SDS sample buffer, incubated for 5min at 95°C and subjected to SDS-PAGE.

## 6.12   Pull down experiments

To isolate AChRs, muscle cell lysate aliquots of 500 $\mu$l were thawed from -80°C on ice and incubated with biotin-conjugated $\alpha$-BTX for 1 hr at 4°C. Afterwards, 20 $\mu$l streptavidin-coupled agarose beads were added and samples were incubated for 1 hr at 4°C on a rotating device. Lysates were centrifuged for 1.5 min at maximum speed in an Eppendorf 5415 D centrifuge. Streptavidin-coupled agarose beads were washed 3 times using 1 ml RIPA lysis buffer containing protease inhibitors. Bound proteins were eluted with SDS sample buffer and subjected to SDS-PAGE.

## 6.13   Immunofluorescence microscopy

Transiently transfected HeLa cells, cultured on glass coverslips (20mm diameter) were washed three times with cold PBS and surface MuSK-SBP receptors were stained for 30min at 4°C with SA-Cy3 or SA-Alexa 594. After staining, cells were washed 3X with cold PBS to remove the free fluorophore and incubated for different time intervals at 37°C in DMEM to let endocytosis to occur. Afterwards cells were washed again in cold PBS and stained for 30min at 4°C with SA-Cy5 or SA-Alexa 488. Cells were washed and fixed with 4% PFA in PBS for 10min at RT. After fixation, PBS washing was repeated and coverslips were mounted onto glass slides in Vectashield mounting medium, sealed with nail polish and viewed on a fluorescence microscope using different excitation wavelengths.

Muscle cells were cultivated on 3.5 cm dishes. Plates were washed at room temperature with PBS and fixed with 4% PFA in PBS for 10min at RT. After fixation, PBS washing was repeated and cells were stained with Alexa-594 conjugated $\alpha$-Bungarotoxin for 60 min for 60min. Cells were washed in PBS to remove the unbound fluorophor and fixed with 4% PFA in PBS for 10min at RT. After another three washing steps with PBS, coverslips and Vectashield mounting medium were used to stabilize the sampels. Coverslips were sealed with nail polish and sampels were visualised with a fluorescent microscope.

In order to specifically label endocytic compartments as the EEA1 early endosomes in muscle cells, C3.16/MuSK-SBP myotubes were first fixed with 4% PFA in PBS for 15min at RT. After fixation, cells were washed in PBS and treated with 0.1mM glycine in PBS for 10min. For permeabilization, cells were incubated with 0.2% Triton in PBS for 10min at RT. Cells were washed 2 times in PBS and then blocked in blocking solution (10% FBS in PBS) for 30min at RT. Then, the cells were incubated with anti-EEA1 antibody diluted with blocking solution for 1 hours at RT. Afterwards, cells were washed three times

with PBS, blocked for 20 min in blocking solution and incubated with species-specific secondary fluorophore-conjugated antibodies diluted in blocking solution for 1 hour at RT. Cells were washed in PBS for 5 minutes on a shaker and mounted in Vectashield mounting medium. Sampels were visualized with a fluorescence microscope.

## 6.14 Quantification of AChR clusters

Quantification of the AChR cluster length and number was done using the Metamorph Imaging Software (Molecular Devices). At least 10 pictures of AChR clusters on the surface of myotubes were taken, from random chosen fields, using the 63x objective. The AChR cluster length was determined by applying a line across the cluster using the free hand tool of the software. The length as well the number of all marked AChR clusters was automatically calculated using "'region measurements"' function of the software. Clusters smaller then 2 $\mu$m were excluded from the statistical analysis. Data was imported and processed with Microsoft Excel Software.

# 6.15   Solutions and buffers

10xTBS-Tween:         100mM Tris.Cl pH8
                      1.5M NaCl
                      0.5 % Tween 20


10xPBS:               1.37M NaCl
                      27mM KCl
                      43mM Na2HPO4
                      14mM KH2PO4


4xSDS Loading Buffer: 240mM Tris.Cl pH6.8
                      8% -Mercaptoethanol
                      8% SDS
                      40% glycerol, bromphenol blue


50xTAE:               242g Tris base
                      57.1ml acetic acid
                      100ml 0.5M EDTA
                      volume adjusted to 1l with dH2O


4% PFA:               0.8g PFA were dissolved in 20ml 1xPBS
                      100 $\mu$l 0.5M NaOH to reach pH7
                      The solution was gently heated and stirred until clear

# Chapter 7

# Abbreviations

| | |
|---|---|
| APS | ammoniumperoxidisulfate |
| ATP | adenosine triphosphate |
| bp | base pair |
| BLAST | basic local alignment research tool |
| BBS | BES buffered saline |
| BES | N,N-bis(2-hydroxyethyl)-2-aminoethanesulfonic acid |
| BLAST | basic local alignment research tool |
| BSA | bovine serum albumin |
| Da | Dalton |
| DMEM | Dulbeco's Modified Eagles Medium |
| DMSO | dimethylsulfoxide |
| dNTPs | deoxyribonucleoside triphosphates |
| EDTA | ethylenediaminetetraacetate |
| EtBr | ethidium bromide |
| FBS | fetal bovine serum |
| GEF | guanine nucleotide exchange factor |
| GFP | green fluorescent protein |
| hr | hour |
| HEPES | 2-[4-(2-Hydroxyethyl)-1-piperazinyl]-ethanesulphonic acid |
| kb | kilobase |

| | |
|---|---|
| kDa | kiloDalton |
| min | minute |
| NP-40 | Nonidet P-40 |
| nt | nucleotide |
| oligo | oligonucleotide |
| PAGE | polyacrylamide gel electrophoresis |
| PBS | phosphate-buffered saline |
| PFA | paraformaldehyde |
| PMSF | phenylmethylsulfonylfluoride |
| pTyr | phosphotyrosine |
| RT | room temperature |
| SDS | sodium dodecyl sulfate |
| sec | second |
| TAE | tris-acetate-EDTA |
| TBS | tris-buffered saline |
| TBE | tris-borate-EDTA |
| TE | tris-EDTA |
| TEA | triethanolamine acetate |
| TEMED | N,N,N,N-tetramethylethylene diamine |
| Tris | tris (hydroxymethyl) aminomethane |

# Bibliography

[Altschuler et al., 1998] Altschuler, Y., Barbas, S., Terlecky, L., Tang, K., Hardy, S., Mostov, K. & Schmid, S. (1998).

[Ando et al., 1994] Ando, A., Yonezawa, K., Gout, I., Nakata, T., Ueda, H., Hara, K., Kitamura, Y., Noda, Y., Takenawa, T., Hirokawa, N. et al. (1994). The EMBO Journal 13, 3033.

[Benmerah et al., 1998] Benmerah, A., Lamaze, C., Begue, B., Schmid, S., Dautry-Varsat, A. & Cerf-Bensussan, N. (1998). Journal of Cell Biology 140, 1055–1062.

[Bezakova & Ruegg, 2003] Bezakova, G. & Ruegg, M. (2003). Nature Reviews Molecular Cell Biology 4, 295–309.

[Blaikie et al., 1994] Blaikie, P., Immanuel, D., Wu, J., Li, N., Yajnik, V. & Margolis, B. (1994). Journal of Biological Chemistry 269, 32031–32034.

[Bloch, 1979] Bloch, R. (1979). The Journal of Cell Biology 82, 626–643.

[Bonifacino et al., 1998] Bonifacino, J., Cao, H., Garcia, F. & McNiven, M. (1998). Molecular Biology of the Cell 9, 2595–2609.

[Brugge et al., 2001] Brugge, J., Burke, P., Schooler, K. & Wiley, H. (2001). Molecular Biology of the Cell 12, 1897–1910.

[Burden, 2002] Burden, S. (2002). J Neurobiol 53, 501–11.

[Burgess et al., 1999] Burgess, R., Nguyen, Q., Son, Y., Lichtman, J., Sanes, J. et al. (1999). NEURON-CAMBRIDGE MA- 23, 33–44.

[Cartaud et al., 2000] Cartaud, J., Cartaud, A., Kordeli, E., Ludosky, M., Marchand, S. & Stetzkowski-Marden, F. (2000). MICROSCOPY RESEARCH AND TECHNIQUE 49, 73–83.

[Ceresa & Schmid, 2000] Ceresa, B. & Schmid, S. (2000). Current Opinion in Cell Biology 12, 204–210.

[Chen et al., 1991] Chen, M., Obar, R., Schroeder, C., Austin, T., Poodry, C., Wadsworth, S. & Vallee, R. (1991). Nature 351, 583–586.

[Chen et al., 1990] Chen, W., Goldstein, J. & Brown, M. (1990). Journal of Biological Chemistry 265, 3116–3123.

[Cheusova et al., 2006] Cheusova, T., Khan, M., Schubert, S., Gavin, A., Buchou, T., Jacob, G., Sticht, H., Allende, J., Boldyreff, B., Brenner, H. et al. (2006). Genes & Development 20, 1800.

[Cohen et al., 1997] Cohen, I., Rimer, M., Lømo, T. & McMahan, U. (1997). Molecular and Cellular Neuroscience 9, 237–253.

[Cook et al., 1996] Cook, T., Mesa, K. & Urrutia, R. (1996). Journal of Neurochemistry 67, 927.

[Cook et al., 1994] Cook, T., Urrutia, R. & McNiven, M. (1994). Proceedings of the National Academy of Sciences 91, 644–648.

[Damke, 1995] Damke, H. (1995). The Journal of Cell Biology 131, 69–80.

[DeChiara, 1996] DeChiara, T. e. a. (1996). Cell 85, 501–512.

[Di Guglielmo et al., 2003] Di Guglielmo, G., Le Roy, C., Goodfellow, A. & Wrana, J. (2003). Nature Cell Biology 5, 410–421.

[Fambrough, 1979] Fambrough, D. (1979).

[Finn et al., 2003] Finn, A., Feng, G. & Pendergast, A. (2003). Nature Neuroscience 6, 717–723.

[Fischbach & Cohen, 1973] Fischbach, G. & Cohen, S. (1973). Dev Biol 31, 147–62.

[Gautam et al., 1996] Gautam, M., NOAKES, P., MOSCOSO, L., RUPP, F., SCHELLER, R., MERLIE, J. & SANES, J. (1996). Cell(Cambridge) 85.

[Glass et al., 1996] Glass, D., Bowen, D., Stitt, T., Radziejewski, C., Bruno, J., Ryan, T., Gies, D., Shah, S., Mattsson, K., Burden, S. et al. (1996). Cell 85, 513–23.

[Guha et al., 2003] Guha, A., Sriram, V., Krishnan, K. & Mayor, S. (2003). Journal of Cell Science 116, 3373–3386.

[Herbst & Burden, 2000] Herbst, R. & Burden, S. (2000). The EMBO Journal 19, 67–77.

[Heuser, 1989] Heuser, J. (1989). The Journal of Cell Biology 108, 389–400.

[Hinshaw, 2000] Hinshaw, J. (2000). Annual Reviews in Cell and Developmental Biology 16, 483–519.

[Huber et al., 2001] Huber, M., Brabec, M., Bayer, N., Blaas, D. & Fuchs, R. (2001). Traffic 2, 727–736.

[Jennings & Burden, 1993] Jennings, C. & Burden, S. (1993). Curr Opin Neurobiol 3, 75–81.

[Kavanaugh & Williams, 1994] Kavanaugh, W. & Williams, L. (1994). Science 266, 1862–1865.

[Keefe et al., 2001] Keefe, A., Wilson, D., Seelig, B. & Szostak, J. (2001). Protein Expression and Purification 23, 440–446.

[Kim et al., 2008] Kim, N., Stiegler, A., Cameron, T., Hallock, P., Gomez, A., Huang, J., Hubbard, S., Dustin, M. & Burden, S. (2008). Cell .

[Lee et al., 1967] Lee, C., Tseng, L. & Chiu, T. (1967). Nature 215, 1177–1178.

[Lin et al., 2001] Lin, W., Burgess, R., Dominguez, B., Pfaff, S., Sanes, J. & Lee, K. (2001). Nature 410, 1057–1064.

[Lu et al., 2008] Lu, J., He, Z., Fan, J., Xu, P. & Chen, L. (2008). Biochemical and Biophysical Research Communications 371, 315–319.

[Luo et al., 2003] Luo, Z., Je, H., Wang, Q., Yang, F., Dobbins, G., Yang, Z., Xiong, W., Lu, B. & Mei, L. (2003). Neuron 40, 703–717.

[Luo et al., 2002] Luo, Z., Wang, Q., Zhou, J., Wang, J., Luo, Z., Liu, M., He, X., Wynshaw-Boris, A., Xiong, W., Lu, B. et al. (2002). Neuron 35, 489–505.

[Ma et al., 2003] Ma, L., Huang, Y., Pitcher, G., Valtschanoff, J., Ma, Y., Feng, L., Lu, B., Xiong, W., Salter, M., Weinberg, R. et al. (2003). Journal of Neuroscience 23, 3164.

[Macia et al., 2006] Macia, E., Ehrlich, M., Massol, R., Boucrot, E., Brunner, C. & Kirchhausen, T. (2006). Developmental Cell 10, 839–850.

[Marmor & Yarden, 2004] Marmor, M. & Yarden, Y. (2004). Oncogene 23, 2057–2070.

[Marshall, 1995] Marshall, C. (1995). Cell 80, 179–85.

[Mayor & Pagano, 2007] Mayor, S. & Pagano, R. (2007). NATURE REVIEWS MOLECULAR CELL BIOLOGY 8, 603.

[McCann et al., 2005] McCann, C., Bareyre, F., Lichtman, J. & Sanes, J. (2005). BIOTECHNIQUES 38, 945.

[McMahan, 1990] McMahan, U. (1990). In Cold Spring Harbor symposia on quantitative biology vol. 55, pp. 407–418, Cold Spring Harbor Laboratory Press.

[Mousavi et al., 2004] Mousavi, S., Malerød, L., Berg, T. & Kjeken, R. (2004). Biochemical Journal 377, 1.

[Mukherjee et al., 2006] Mukherjee, S., Tessema, M. & Wandinger-Ness, A. (2006). Circulation Research 98, 743–756.

[Nakata, 1993] Nakata, T. (1993).

[Newman-Smith et al., 1997] Newman-Smith, E., Shurland, D. & van der Bliek, A. (1997). Genomics 41, 286–289.

[Nitkin, 1987] Nitkin, R. (1987). The Journal of Cell Biology 105, 2471–2478.

[Numberger et al., 1991] Numberger, M., Dürr, I., Kues, W., Koenen, M. & Witzemann, V. (1991). The EMBO Journal 10, 2957.

[Okada et al., 2006] Okada, K., Inoue, A., Okada, M., Murata, Y., Kakuta, S., Jigami, T., Kubo, S., Shiraishi, H., Eguchi, K., Motomura, M. et al. (2006).

[Owen et al., 2004] Owen, D., Collins, B. & Evans, P. (2004). Annual Review of Cell and Developmental Biology 20, 153–191.

[Paratcha & Ibáñez, 2002] Paratcha, G. & Ibáñez, C. (2002). Current Opinion in Neurobiology 12, 542–549.

[Pato et al., 2008] Pato, C., Stetzkowski-Marden, F., Gaus, K., Recouvreur, M., Cartaud, A. & Cartaud, J. (2008). Chemico-Biological Interactions .

[Ruegg & Bixby, 1998] Ruegg, M. & Bixby, J. (1998). Trends in Neurosciences 21, 22–27.

[Sadasivam et al., 2005] Sadasivam, G., Willmann, R., Lin, S., Erb-Vogtli, S., Kong, X., Ruegg, M. & Fuhrer, C. (2005). Journal of Neuroscience 25, 10479.

[Salpeter et al., 1993] Salpeter, M., ANDREOSE, J., O'MALLEY, J., XU, R., FUMAGALLI, G. & LOMO, T. (1993). Annals of the New York Academy of Sciences 681, 155–164.

[Sanes, 1978] Sanes, J. (1978). The Journal of Cell Biology 78, 176–198.

[Sanes & Lichtman, 2001] Sanes, J. & Lichtman, J. (2001). Nat Rev Neurosci 2, 791–805.

[Scaife, 1990] Scaife, R. (1990). The Journal of Cell Biology 111, 3023–3033.

[Scaife et al., 1994] Scaife, R., Gout, I., Waterfield, M. & Margolis, R. (1994). The EMBO Journal 13, 2574.

[Schafer, 2004] Schafer, D. (2004). Traffic 5, 463–469.

[Seedorf et al., 1994] Seedorf, K., Kostka, G., Lammers, R., Bashkin, P., Daly, R., Burgess, W., van der Bliek, A., Schlessinger, J. & Ullrich, A. (1994). Journal of Biological Chemistry 269, 16009–16014.

[Sigismund et al., 2005] Sigismund, S., Woelk, T., Puri, C., Maspero, E., Tacchetti, C., Transidico, P., Di Fiore, P. & Polo, S. (2005). Proceedings of the National Academy of Sciences 102, 2760–2765.

[Suzuki et al., 2004] Suzuki, S., Numakawa, T., Shimazu, K., Koshimizu, H., Hara, T., Hatanaka, H., Mei, L., Lu, B. & Kojima, M. (2004). The Journal of Cell Biology .

[Thompson & McNiven, a] Thompson, H. & McNiven, M. .

[Tsen et al., 1995] Tsen, G., Halfter, W., Kröger, S. & Cole, G. (1995). Journal of Biological Chemistry 270, 3392.

[Urrutia et al., 1997] Urrutia, R., Henley, J., Cook, T. & McNiven, M. (1997). Proceedings of the National Academy of Sciences 94, 377–384.

[Valenzuela et al., 1995] Valenzuela, D., Stitt, T., DiStefano, P., Rojas, E., Mattsson, K., Compton, D., Nunez, L., Park, J., Stark, J., Gies, D. et al. (1995). Neuron 15, 573–584.

[Vieira et al., 1996] Vieira, A., Lamaze, C. & Schmid, S. (1996). Science 274, 2086.

[Vogel et al., 1972] Vogel, Z., Sytkowski, A. & Nirenberg, M. (1972). Proceedings of the National Academy of Sciences 69, 3180–3184.

[Wang et al., 2004] Wang, Y., Pennock, S., Chen, X., Kazlauskas, A. & Wang, Z. (2004). Journal of Biological Chemistry 279, 8038.

[Watty et al., 2000] Watty, A., Neubauer, G., Dreger, M., Zimmer, M., Wilm, M. & Burden, S. (2000).

[Weatherbee et al., 2006] Weatherbee, S., Anderson, K. & Niswander, L. (2006). Development 133, 4993.

[Xu & Salpeter, 1997] Xu, R. & Salpeter, M. (1997). Journal of Neuroscience 17, 8194–8200.

[Yang et al., 2005] Yang, X., Huang, Y., Xiong, W. & Mei, L. (2005). Molecular and Cellular Neuroscience 28, 335–346.

[Zhang et al., 2008] Zhang, B., Luo, S., Wang, Q., Suzuki, T., Xiong, W. & Mei, L. (2008). Neuron 60, 285–297.

[Zhu et al., 2006] Zhu, D., Xiong, W. & Mei, L. (2006). Journal of Neuroscience 26, 4841.

[Zhu et al., 2008] Zhu, D., Yang, Z., Luo, Z., Luo, S., Xiong, W. & Mei, L. (2008). Journal of Neuroscience 28, 1688.

# Lebenslauf

| | |
|---|---|
| **Name** | Cristina Melinte |
| **Geburtstag** | 5 Iulie 1980 |
| **Nationalit**ät | Rumänisch |

**Schul- und Berufsbildung**

| | |
|---|---|
| **1995-1999** | "Mihai Viteazul", Gymnasium Oberstufe, Ploiesti/ Rumänien |
| **1999-2001** | Studium der Humanmedizin an der Universität Targu-Mures |
| **2001-2005** | Studium der Biologie an der Universität Bukarest, |
| | Abschluss als Bachelor der Naturwissenschaften mit Auszeichnung |
| **SS 2007-SS 2009** | Diplomstudium der Biologie an der Universität Wien |
| **Sept 2007-Nov 2008** | Vom FWF geförderte Diplomarbeit am Hirnforschungsinstitut der |
| | Medizinischen Universität Wien; Thema:"Characterization of MuSK |
| | endocytosis at the neuromuscular junction" |